# Microvascular and systemic effects following top load administration of saturated carbon monoxide-saline solution*

Nanae Hangai-Hoger, MD, PhD; Amy G. Tsai, PhD; Pedro Cabrales, PhD; Makoto Suematsu, MD, PhD; Marcos Intaglietta, PhD

*Objective:* To determine how top loads with different doses of carbon monoxide (CO)-saturated saline solutions (CO-saline) affect microvascular and systemic hemodynamics and to delineate the corresponding biochemical mechanisms.

*Design:* Prospective study.

*Setting:* University research laboratory.

*Subjects:* Male Golden Syrian hamsters.

*Interventions:* Hamsters implemented with a dorsal window chamber were given different volumes (characterized as percent of blood volume, BV) by intravenous injection of CO-saturated saline.

*Measurements and Main Results:* Hamsters were observed until 90 mins after infusion of CO-saline solution. In the 20% BV CO-saline infusion group, observation was extended until 180 mins. Systemic variables measured included mean arterial pressure, heart rate, systemic arterial blood gases, and cardiac output and index. Microvascular hemodynamic measurements included vessel diameter, red blood cell velocity, and functional capillary density. Cyclic guanosine monophosphate (cGMP) content in the chamber tissue was measured by enzyme immunoassay. 10% BV of CO-saline increased flow maximally in the microcirculation at 30 mins after infusion (207% in arterioles and 238% in venules, $p < .05$ vs. baseline). Functional capillary density was significantly increased in both 10% and 15% groups ($p < .05$ vs. baseline), and cardiac index increased 130% ($p < .05$ vs. baseline) at 10 mins after 10% CO-saline infusion. There were no changes of microhemodynamic variables and functional capillary density with 2.5%, 5%, and 20% CO-saline infusion during the observation period. Microvascular hemodynamic changes by 10% CO-saline infusion were inhibited completely by L-NAME pretreatment and partially by 1H-[1,2,4]oxadiazole[4,3-a]quinoxqalin-1-one pretreatment. cGMP content in skin fold tissues was related to changes of vessel diameter.

*Conclusions:* Intravenous injection of CO-saturated saline caused vasodilation and improved microvascular hemodynamics in the hamster window chamber model in a dose-dependent manner. These changes were related to increased cardiac output and local cGMP content. These results support the possible use of CO-saturated solutions as a vasodilator in critical conditions. (Crit Care Med 2007; 35:1123–1132)

KEY WORDS: carbon monoxide; vasodilatation; microcirculation; cyclic guanosine monophosphate; cardiac output; hamster window model

Carbon monoxide (CO) binds to soluble guanylate cyclase (sGC) to increase cyclic guanosine monophosphate (cGMP) in vascular tissue, causing vascular relaxation. Both inhalation and intraperitoneal injection of CO gas cause cardiovascular effects, lowering mean arterial blood pressure (MAP), increasing heart rate (HR), increasing cardiac output, and decreasing total peripheral vascular resistance (1, 2). These effects are present upon the introduction of CO when CO-hemoglobin (CO-Hb) saturation is as low as 7%.

CO is toxic at high dosages and is an effective vasodilator at low dosages that protects cellular species from ischemic damage and inflammation. Its multiple effects suggest that it should be beneficial in the acute treatment of ischemic heart disease, microcirculatory impairment, and ischemic shock. In emergencies requiring blood transfusion, plasma expanders are used until appropriate blood becomes available. In this situation, systemic blood pressure, HR, and respiratory rate are frequently in the normal range while the microcirculation is impaired, a condition not evident from systemic variables. The initial microvascular impairment begins with the decrease of functional capillary density (FCD) (3); the rapid reversal of this process and improvement of microvascular flow are necessary for impeding the progression of irreversible organ damage.

This situation suggests the development of a plasma expander with flow-increasing properties beyond those afforded by the decrease in blood viscosity due to hemodilution. Nitric oxide (NO) is a well-known vasodilator, although it is short lasting. Since endogenous CO functions as a vasodilator, exogenous CO could in principle provide the required vasodilator effect with temporal advantage. Inhalation of CO or intraperitoneal injection of CO gas was beneficial (1, 2); however, these procedures do not lend themselves to accurate dosage. We propose that the intravenous injection of

*See also p. 1213.

From the Department of Bioengineering, University of California, San Diego, La Jolla, CA (NHH, AGT, MI); La Jolla Bioengineering Institute, La Jolla, CA (AGT, PC, MI); and Department of Biochemistry & Integrative Medical Biology, School of Medicine, Keio University, Tokyo, Japan (MS).

Supported, in part, by USPHS Bioengineering Research Partnership grant R24-HL64395, by grants R01-HL62354 and R01-HL62318 (MI), and by Leading Project for Biosimulation from the Ministry of Education, Sciences and Technology of Japan (MS).

The authors have not disclosed any potential conflicts of interest.

For information regarding this article, E-mail: nhangai@bioeng.ucsd.edu



DOI: 10.1097/01.CCM.0000259533.84180.C7

CO-saturated saline (CO-saline) provides a practical and readily quantifiable method for delivering CO to the organism with the aim of increasing microvascular perfusion.

To test our hypothesis, we infused CO-saline solution as top loads to the hamster window chamber model, in different percentages of blood volume, to establish the extent and duration of microvascular and systemic responses and then determine the effectiveness of this methodology in producing dose-dependent vasodilation. In addition, we studied the effects of CO-saline during L-NAME and the sGC inhibitor 1H-[1,2,4]oxadiazole[4,3-a]quinoxqalin-1-one (ODQ) treatment to delineate the corresponding biochemical pathways.

## MATERIALS AND METHODS

### Animal Preparation

Investigations were performed in male Golden Syrian hamsters (Charles River Laboratories, Boston, MA) according to the procedures outlined in the *Guide for the Care and Use of Laboratory Animals* (National Research Council, 1996) and were approved by the local animal subjects committee. The hamster window chamber model is widely used for microvascular studies in the unanesthetized state, and the complete surgical technique is described elsewhere (4). Catheters (PE-50) were implanted in the carotid artery and jugular vein. Experiments were performed after at least 24 hrs but within 48 hrs after catheter implantation. Both procedures were performed under anesthesia (Nembutal, 50 mg/kg, intraperitoneal injection, Abbott, Abbott Park, IL).

### Systemic Variables

MAP was tracked continuously during the experimental period, and HR was determined from the pressure trace (Biopac, Santa Barbara, CA; Spectramed Pressure Transducer). Hematocrit was measured from centrifuged arterial blood samples taken in heparinized capillary tubes.

### Blood Chemistry

Arterial blood was sampled from the carotid artery catheter into heparinized capillary tubes and immediately analyzed for $P_{O_2}$, $P_{CO_2}$, and pH at 37 EC (pH/Blood Gas Analyzer, 248, Bayer). Hemoglobin concentration was measured using a photometer (B-Hemoglobin, Hemocue, Sweden).

### Microhemodynamic Variables

The unanesthetized animal was placed in a restraining tube attached to the stage of an inverted microscope (IMT-2 Olympus, New Hyde Park, NY) equipped with ×20 objective (Leitz PHARCO L1, n.a. 0.32). The tissue image was projected onto a CCD camera (COHU 4815-2000, COHU, San Diego, CA), video recorded (Panasonic AG-7355,) and viewed on a Sony monitor (PVM-1271Q).

*Microhemodynamics.* Arteriolar and venular blood flow velocities were measured using the photodiode cross-correlation method (5) (Photo Diode/Velocity Tracker 102B, Vista Electronics, San Diego, CA). The measured centerline velocity ($V$) was corrected according to vessel size to obtain mean red blood cell (RBC) velocity (6). A video image-shearing method was used to measure vessel diameter ($D$) (7). Blood flow ($Q$) was calculated from the measured values as $Q = V\,\mathrm{H}\,B(D/2)^2$.

*Arterioles and Venules.* Microvessels were classified according to their position in the microvascular network (3) including large feeding arterioles, small arcading arterioles, large venules, and small collecting venules (8).

*Functional Capillary Density.* Capillaries are considered functional if RBCs transit through the capillary segments during a 45-sec period. FCD was tabulated from the capillary lengths with RBC transit in an area comprising ten successive microscopic fields (420 × 320 $\mu m^2$).

### Saturated CO-Saline Solution

Normal saline (0.9% NaCl) was bubbled with 100% CO (Airgas, Radnor, PA) for 20 mins at room temperature and atmospheric pressure resulting in a concentration of about $0.93 \times 10^{-4}$ M (CO = 28.01 molecular weight and 0.0026 g/100 mL solubility in water at 20°C) and a maximal possible HbCO concentration of 1% for a 10% top load.

### Circulatory Carboxy Hemoglobin Concentration

CO-Hb concentration in systemic venous blood was measured spectrophotometrically according to Parks and Worth (9). The second derivative spectrum was determined between 390 and 450 nm using a UV/VIS Spectrometer (Lambda 20, Perkin Elmer, Wellesley, MA), and data were analyzed using the standard curve from normal hamster samples.

### cGMP Content in the Skin Fold

Concentration of cGMP in the skin tissue was determined using a commercial enzyme immunoassay kit (Enzymeimmunoassay Biotrak System, Amersham Biosciences, Piscataway, NJ). Tissues were snap-frozen in liquid nitrogen immediately after dissection from the anesthetized animals. Samples were stored at −80°C until analysis. Assays were per-

Table 1. Mean arterial pressure (MAP) and heart rate (HR) as a function of the amount of carbon monoxide (CO)-saline delivered by top load

| | No. | BL | 10 Mins | 30 Mins | 60 Mins | 90 Mins |
|---|---|---|---|---|---|---|
| MAP, mm Hg | | | | | | |
| 10% TP | 4 | 112 ± 10 | 112 ± 14 | 116 ± 16 | 110 ± 7 | 114 ± 11 |
| 20% TP | 4 | 121 ± 8 | 122 ± 12 | 117 ± 5 | 117 ± 6 | 114 ± 5 |
| 2.5% CO | 5 | 110 ± 8 | 111 ± 8 | 109 ± 6 | 107 ± 8 | 106 ± 9 |
| 5% CO | 4 | 120 ± 15 | 121 ± 13 | 119 ± 11 | 119 ± 14 | 118 ± 14 |
| 10% CO | 5 | 115 ± 9 | 113 ± 9 | 112 ± 10 | 109 ± 9 | 107 ± 6[a] |
| 15% CO | 5 | 112 ± 11 | 107 ± 12 | 103 ± 9[a] | 100 ± 7[a] | 103 ± 7[a] |
| 20% CO | 4 | 112 ± 3 | 110 ± 1 | 107 ± 5 | 107 ± 6 | 108 ± 6 |
| HR, beats/min | | | | | | |
| 10% TP | 4 | 404 ± 8 | 387 ± 10 | 397 ± 28 | 408 ± 22 | 413 ± 33 |
| 20% TP | 4 | 412 ± 50 | 381 ± 42 | 388 ± 37 | 383 ± 33 | 389 ± 33 |
| 2.5% CO | 5 | 412 ± 22 | 423 ± 27 | 426 ± 9 | 413 ± 18 | 412 ± 30 |
| 5% CO | 4 | 388 ± 21 | 386 ± 50 | 405 ± 58 | 434 ± 27 | 400 ± 37 |
| 10% CO | 5 | 443 ± 27 | 421 ± 32 | 427 ± 34 | 429 ± 29 | 414 ± 45 |
| 15% CO | 5 | 429 ± 52 | 396 ± 60 | 406 ± 44 | 359 ± 51 | 364 ± 15 |
| 20% CO | 4 | 431 ± 54 | 420 ± 53 | 420 ± 52 | 415 ± 53 | 404 ± 36 |

BL, baseline; 10% TP, top load of 10% blood volume of saline (= 0% CO); 20% TP, top load 20% blood volume of saline.
[a] $p < .05$ vs. baseline.

formed according to the manufacturer's protocol.

## Experimental Protocol

*Systemic and Microvascular Effects of CO.* Thirty-five animals were entered for systemic MAP and HR and microvascular studies (body weight [BW] 57.5 ± 5.8 g, range 49.6–75.0 g). Blood volume (BV) was estimated at 7% of BW. Preliminary experiments determined that 10% or 20% saline top loads (n = 4 each) caused no systemic effects. Animals were divided into six groups: a) 0%, receiving 10% BV of saline (n = 4); b) 2.5%, receiving 2.5% BV of CO-saline (n = 5); c) 5%, receiving 5% BV of CO-saline (n = 4); d) 10%, receiving 10% of blood volume of CO-saline (n = 5); e) 15%, receiving 15% of blood volume of CO-saline (n = 5); and f) 20%, receiving 20% BV of CO-saline (n = 4). In the 2.5% and 5% groups, infusion volume was adjusted to 10% BV with 0.9% saline solution. Solutions were infused intravenously at the rate of 5% BV per minute. Measurements were made 10, 30, 60, and 90 mins after infusion. Four additional animals in the 20% group were observed at 120, 150, and 180 mins.

*CO Effect on Cardiac Output.* Ten animals were entered for this study (BW = 115.5 ± 20.9 g, range 63.0–136.0 g). Cardiac output was measured by thermodilution (10) in the 0% (n = 5) and 10% groups (n = 5). These animals had a greater BW to facilitate catheter placement.

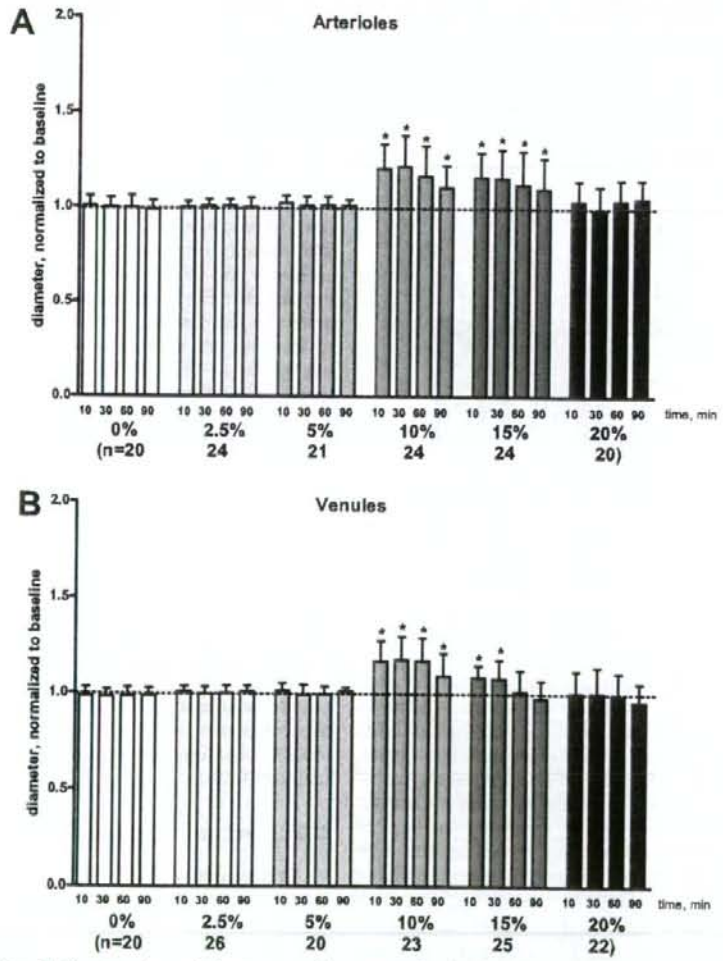


Figure 1. Changes of vessel diameters are shown normalized to baseline. Broken line represents baseline level (BL). *A*, changes of arteriolar diameter. In the 10% and 15% group, carbon monoxide (CO) caused a significant vasodilatory effect during the period of observation (*$p < .05$ vs. BL). *B*, changes of venular diameter. CO caused a significant vasodilatory effect in the 10% and 15% groups. This effect was significantly greater in the 10% group than in 15% group (†$p < .05$ vs. 15%).

*Effect of NO Synthase Inhibitor L-NAME.* Nine animals were entered for this study (BW = 59.2 ± 6.9 g, range 51.0–69.0 g). The effect of the nonselective NO synthase (NOS) inhibition was studied by administering intravenously 30 mg·kg$^{-1}$ L-NAME (Sigma, St. Louis, MO) 30 mins before infusion of 10% CO-saline (11). Animals were randomly divided into two groups: a) L-NAME-s, L-NAME followed by 10% BV saline top load (n = 4); and b) L-NAME-CO, L-NAME followed by 10% BV CO-saline top load (n = 5). Measurements were made 30 mins after administration of L-NAME and 10, 30, 60, and 90 mins after the intravenous infusion of CO-saline.

*Effect of sGC Inhibitor ODQ.* Eighteen animals were entered for this study (BW = 61.1 ± 8.7 g, range 51.0–77.5 g). The effect of CO on the sGC-cGMP pathway was analyzed following the intravenous administration of 10 g·kg$^{-1}$ of ODQ (Sigma) 30 mins before infusion of 10% CO-saline (12). ODQ was dissolved in dimethyl sulfoxide (DMSO) and diluted with 0.9% saline to a final DMSO concentration of about 0.04%. Animals were randomly divided into four groups: a) DMSO-s, 0.04% DMSO vehicle followed by 10% BV saline (n = 4); b) DMSO-CO, 0.04% DMSO vehicle followed by 10% BV of CO-saline (n = 5); c) ODQ-s, ODQ followed by 10% BV saline top load (n = 4); and d) ODQ-CO, ODQ followed by 10% BV of CO-saline (n = 5). Measurements were as in the L-NAME treatment experiment.

*cGMP Content in the Skin Chamber Tissue.* Thirty-one animals were entered for this study (BW = 65.7 ± 7.5 g, range 55.5–89.0 g). cGMP content was studied in the following groups: a) control, no treatment (n = 5); b) 10%, CO-saline (n = 5); c) 20% CO-saline (n = 4); d) L-NAME-s and 10% saline (n = 5); e) L-NAME-CO, L-NAME followed by 10% CO-saline (n = 4); f) ODQ-s, ODQ followed by 10% saline (n = 4); and g) ODQ-CO, ODQ followed by 10% BV of CO-saline (n = 4). Tissue was collected from each animal at 30 mins after either saline or CO-saline infusion.

*Experimental Sequence and Data Analysis.* Five studies were performed: a) dose dependency of CO-saline; b) cardiac output; c) NOS inhibition with L-NAME; d) SGC inhibition with ODQ; and g) cGMP content. After dose dependency was established, animals for each of the other studies were randomized to the different treatments groups following the scheme of Altman and Bland (13).

Results are presented as average ± SD unless otherwise noted. Data are presented as absolute values and ratios relative to baseline values. Statistical analysis was performed using one-way and paired analysis of variance when appropriate. *Post hoc* analysis was performed using Newman-Keuls' test between pairs if significance was found. All statistics were calculated by using GraphPad Prism 4.01 (GraphPad Software, San Diego, CA). Changes were considered statistically significant if $p < .05$.

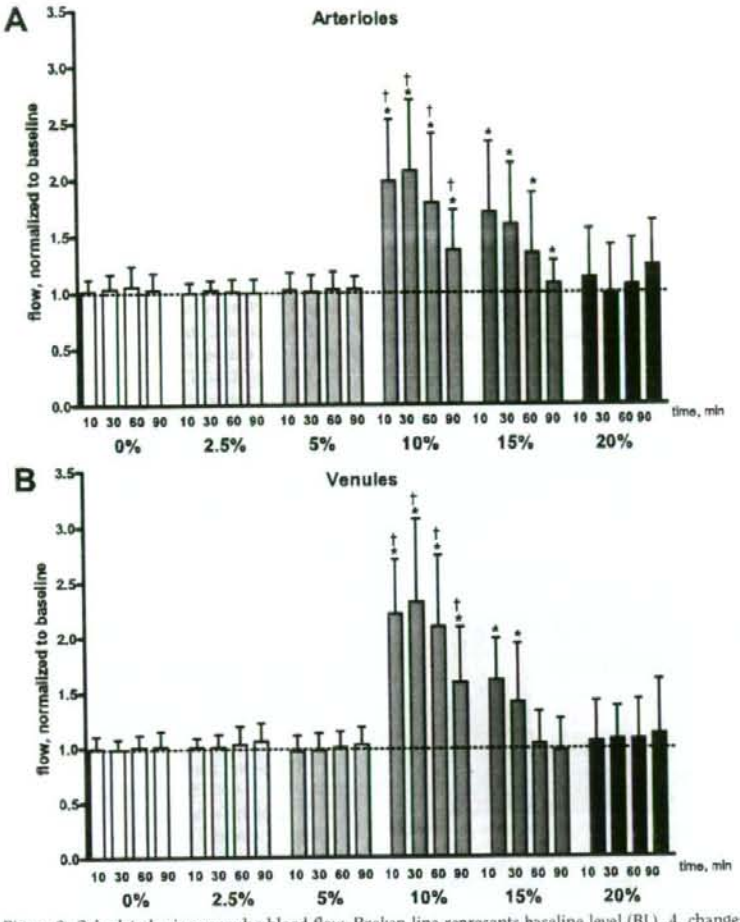


Figure 2. Calculated microvascular blood flow. Broken line represents baseline level (BL). *A*, changes of arteriolar flow. In the 10% and 15% groups, flow was increased significantly after carbon monoxide-saline injection (*$p < .05$ vs. BL). Changes of flow in the 10% group were significantly greater than those in the 15% group at 30, 60, and 90 mins (†$p < .05$ vs. 15%). *B*, changes of venular flow. In the 10% and 15% groups, flow increased significantly vs. baseline (*$p < .05$ vs. BL). Changes of flow in the 10% group were significantly greater than those in the 15% group (†$p < .05$).

## RESULTS

### Systemic and Microvascular Effects of CO-Saline Top Loads

MAP decreased significantly at 30 mins and 60 mins after infusion of CO-saline in the 15% group and at 90 mins in the 10% group. HR did not show significant changes (Table 1). Baseline data were no different among groups.

Saline top loads of 10% or 20% BV did not affect microhemodynamic conditions. There was a slight decrease in HR and microvascular flow; however, these effects were not statistically significant. Increase in arteriolar diameter was statistically significant after CO-saline infusion in the 10% group (maximum at 30 mins, 121%) and the 15% group (maximum at 10 mins, 116%) from baseline, lasting until the end of the observation period (Fig. 1*A*). Increase in venular diameter was statistically significant during the whole observation period in the 10% group (maximum at 30 mins, 118%) and after 10 and 30 mins in the 15% group from baseline (maximum at 10 mins, 109%)(Fig. 1*B*). The calculated upper bound concentration of CO-Hb following the 10% top load injection was 1%.

RBC velocity in both arterioles and venules increased after CO-saline infusion during the entire observation period in the 10% group and at t = 10 and 30 mins in the 15% group. Changes in the 10% group were statistically significantly greater than in the 15% group at 30 and 60 mins in arterioles and during the entire observation period in venules.

Flow increased significantly at all times in the 10% and 15% groups at 10 and 30 mins in arterioles (Fig. 2*A*) and venules (Fig. 2*B*), reaching a maximum at 30 mins. Changes of flow were significantly greater in the 10% group than in the 15% group at 30, 60, and 90 mins in arterioles and at all times in venules.

FCD increased in both the 10% and 15% groups (Fig. 3). The CO effect on FCD lasted until the end of the observation period. There were no significant differences between the 10% and 15% groups.

Since flow still increased at 90 mins in the 20% group, observations were continued to 180 mins after CO-saline infusion using another set of animals (n = 4). Vessel diameter increased significantly at 120 and 150 mins in arterioles and 120 mins in venules after CO-saline injection. RBC velocity increased at 120 mins in arterioles and 90, 120, and 150 mins in venules after CO-saline infusion. In both arterioles and venules, maximal changes of diameter and velocity were the same magnitude as those found in the 15% group. Flow increased at 120 mins in arterioles (Fig. 4*A*) and 90, 120, and 150 mins in venules (Fig. 4*B*) after CO-saline infusion. Maximal changes of flow were at 120 mins and relative values were almost the same as maximal change in the 15% group. FCD did not change during the observation period.

### CO-Hb Concentration in the Systemic Circulation

CO-Hb concentration measured from arterial samples at 10, 30, 60, and 90 mins after infusion in the 10% group (n = 4) was <0.2%, the limit of resolution of the method (9, 13).

### CO Effect on Cardiac Output

Animals were divided into the 0% and 10% groups. Cardiac output increased significantly at 10 mins after CO-saline injection and gradually decreased to baseline levels (Fig. 5). Cardiac index, calculated as cardiac output divided by BW, increased by 31% at 10 mins from baseline in the 10% group vs. 12% in the 0% group.

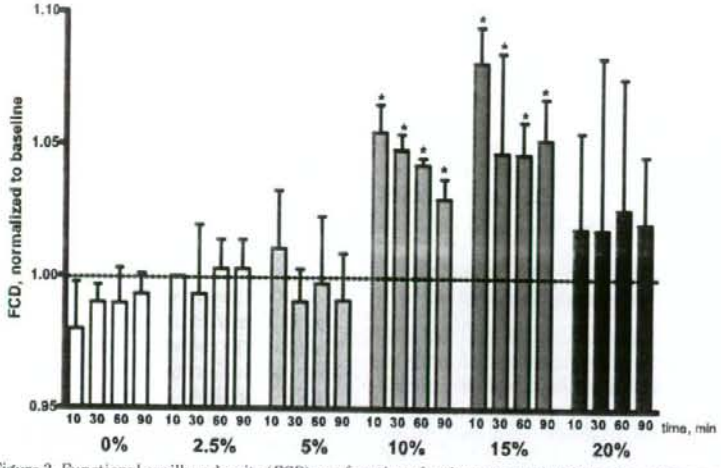


Figure 3. Functional capillary density (*FCD*) as a function of carbon monoxide (CO)-saline delivery and time. Broken line represents baseline level (BL). In the 10% and 15% groups, FCD was significantly increased after CO-saline infusion (*$p < .05$ vs. BL). There was no difference between the 10% and 15% groups.

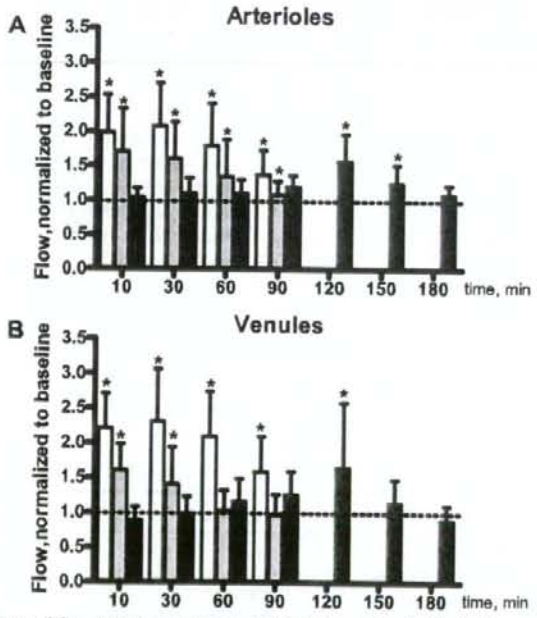


Figure 4. Changes of flow during the extended period of observation in the 20% group (*black bars*) along with 10% (*white bars*) and 15% (*light gray bars*) groups. Broken line represents baseline level (BL). Delayed increase of flow was seen in both arterioles and venules (*$p < .05$ vs. BL).

### Effect of L-NAME

Administration of the nonselective NOS inhibitor L-NAME significantly increased MAP by ~20% and decreased HR by ~40%, an effect that persisted until the end of the observation period in both L-NAME-s and L-NAME-CO groups (Table 2).

In both groups, L-NAME decreased vessel diameter from baseline: arterioles (~14%) and venules (~12%). RBC velocity decreased in both groups in arterioles (~35%) and venules (~24%). In the L-NAME-CO group, arteriolar RBC velocity decreased significantly at 60 and 90 mins after CO-saline infusion. Flow was diminished by about 50% with L-NAME treatment, and 10% CO-saline could not increase flow in arterioles and venues (Fig. 6, *A* and *B*). FCD decreased nearly 30% by L-NAME treatment in both groups (Fig. 6*C*), and 10% CO-saline did not increase FCD. There were no differences between the L-NAME treated groups in any variable at any time points.

### Effect of sGC Inhibitor ODQ

MAP and HR were not changed in the ODQ and DMSO-vehicle groups (Table 2). In the ODQ-CO group, RBC velocity increased at 10 and 30 mins in arterioles and at 30 mins in venules after CO-saline infusion. The DMSO vehicle had no microhemodynamic effects (Fig. 7). CO-saline increased flow significantly in both arterioles and venules at the 30-min time point after ODQ treatment. However, these changes were significantly smaller than in the 10% group (Fig. 7, *A* and 7*B*). At 30 mins after saline infusion, FCD was significantly lower than in the ODQ-treated groups (Fig. 7*C*).

### cGMP Content in the Window Chamber Tissue

Hamster skin cGMP was 2470 ± 810 fmol/g in control and increased to 4860 ± 1550 fmol/g following 10% CO-saline infusion. The basal production of cGMP was not changed by L-NAME or ODQ, and cGMP content followed by 10% CO-saline infusion did not show any differences from control. L-NAME treatment significantly decreased diameter (normal groups), whereas cGMP concentration was lower than control but not significantly different (Fig. 8*A*) although the regression between diameters and for cGMP concentration was significant ($R^2 = .92$, $p < .05$) (Fig. 8*B*).

## DISCUSSION

Our principal finding is that a 10% top load infusion of CO-saturated saline induced microvascular vasodilatory effects lasting up to 90 mins and increased cardiac output and capillary perfusion in the hamster window chamber model. The CO effect was concentration dependent, where 10% BV of CO-saline infusion was the most effective and lasted longer than either lower or higher concentrations. This effect was completely inhibited by L-NAME and partially by ODQ administration.

CO is known as a toxic gas, but this is a matter of dosage. At the effective dosage (10% and 15% top load), the effects in our experiments occurred within 10 mins, and increasing dosage to 20% did not produce an effect. Conversely, Kanten et al. (1) and Gutierrez et al. (2) found effects that were similar to ours after prolonged CO gas inhalation (up to several hours) or intraperitoneal 100% CO gas injection for 102 mins, reaching CO-Hb concentrations ranging from 7.5% to 58%. Therefore, it is likely that the effective dosage seen in our experiments was rapidly exceeded in experiments where CO was delivered by continuous inhalation due to the progressive accumulation of CO in blood. Since effects similar to ours were obtained with ≥10 times CO-Hb dosages by others (1, 2), it would seem that high-dosage CO involves different biochemical processes and pathways than those analyzed in the present work. Guo et al. (14) reported that CO-releasing CORM-3 compound showed effectiveness by intravenous administration when CO reached an estimated blood concentration of 20 μM, and CO-Hb in blood was 0.65% vs. control of 0.53%. They also reported that CO-Hb was virtually undetectable (<1%) until a concentration of ≥200 μM of CORM-3 was achieved *in vivo*.

## CO Effects on the Systemic and Peripheral Circulation

The effects of 10% BV top load of CO-saline should be exclusively due to the presence of CO since there was no evidence of systemic or microvascular effects following a 10% BV of saline top load. MAP decreased significantly after 10% and 15% CO-saline top loads, due to the decrease of vascular resistance consequent to vasorelaxation, observed within 2 mins of injection.

Concentration-dependent effects of CO parallel similar to ours have been reported by Thorup et al (15). Repeated administration of CO was reported to lead to a decline of NO release, and higher concentration of CO inhibited endothelial NOS activity (15–17). Studies also show that CO binds to NOS, inhibiting NO production (18–22), causing vasoconstriction, and increasing blood pressure (23). These opposite observations may be explained by a dose-dependent interaction of CO and NO (24–28). Low concentration of CO causes vasoconstriction in the cerebral microcirculation (29), an effect that could be present in our model; however, 2.5% CO-saline did not show statistically significant changes in systemic and microcirculatory variables when compared with baseline and the 0% CO-saline group.

The 20% CO-saline top load caused microvascular effects similar in magnitude to those following the 15% top load but delayed by 90 mins. This shows that the CO effect on microvessels was maximized at the 10–15% concentration range, and if this range was exceeded, effects began when diffusion decreased concentration of CO.

The addition of CO to the circulating blood provides an additional stimulus to the production of NO, the principal factor in causing vasodilation. However, this mechanism is operational until the concentration of CO inhibits NO production, at which point the vasodilatory stimulus subsides. Our results suggest that once CO inhibits NO production in the endothelium, the recovery process is slow and does not take place during our experiments.

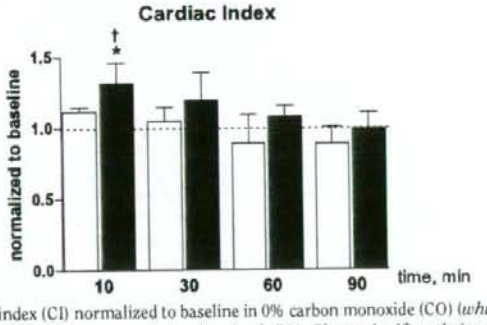


Figure 5. Cardiac index (CI) normalized to baseline in 0% carbon monoxide (CO) (*white bars*) and 10% CO (*black bars*). Broken line represents baseline level (BL). CI was significantly increased at 10 mins after CO-saline infusion (*$p < .05$ vs. BL; †$p < .05$ vs. 0%).

Table 2. Mean arterial pressure (MAP) and heart rate (HR) in L-NAME and 1H-[1,2,4]oxadiazole[4,3-a]quinoxqalin-1-one (ODQ) treatment groups

| | No. | BL | Inhibitor | 10 Mins | 30 Mins | 60 Mins | 90 Mins |
|---|---|---|---|---|---|---|---|
| MAP, mm Hg | | | | | | | |
| 10% CO | 5 | 117 ± 8 | | 117 ± 6 | 115 ± 9 | 112 ± 5 | 109 ± 4 |
| L-NAME | 4 | 110 ± 2 | 132 ± 7[a] | 132 ± 6[a,b] | 133 ± 5[a,b] | 136 ± 3[a,b] | 132 ± 8[a,b] |
| L-NAME-CO | 5 | 115 ± 8 | 141 ± 5[a] | 144 ± 9[a,b] | 143 ± 4[a,b] | 143 ± 7[a,b] | 142 ± 11[a,b] |
| DMSO | 4 | 106 ± 9 | 105 ± 10 | 106 ± 9 | 106 ± 10 | 106 ± 6 | 105 ± 8 |
| DMSO-CO | 5 | 106 ± 8 | 104 ± 6 | 105 ± 8 | 103 ± 10 | 106 ± 10 | 106 ± 10 |
| ODQ | 4 | 103 ± 4 | 103 ± 3 | 100 ± 3 | 99 ± 4 | 100 ± 3 | 98 ± 3 |
| ODQ-CO | 5 | 97 ± 3 | 96 ± 6 | 97 ± 6 | 95 ± 5 | 96 ± 4 | 95 ± 6 |
| HR, beats/min | | | | | | | |
| 10% CO | 5 | 449 ± 27 | | 427 ± 32 | 436 ± 31 | 432 ± 32 | 412 ± 52 |
| L-NAME | 4 | 451 ± 32 | 283 ± 54[a] | 256 ± 81[a,b] | 242 ± 67[a,b] | 243 ± 54[a,b] | 249 ± 47[a,b] |
| L-NAME-CO | 5 | 407 ± 26 | 260 ± 52[a] | 266 ± 47[a,b] | 289 ± 62[a,b] | 252 ± 38[a,b] | 253 ± 23[a,b] |
| DMSO | 4 | 416 ± 22 | 422 ± 28 | 409 ± 36 | 410 ± 16 | 415 ± 21 | 412 ± 18 |
| DMSO-CO | 5 | 427 ± 21 | 422 ± 20 | 425 ± 27 | 425 ± 17 | 427 ± 27 | 419 ± 21 |
| ODQ | 4 | 400 ± 19 | 408 ± 32 | 395 ± 11 | 403 ± 41 | 408 ± 18 | 413 ± 19 |
| ODQ-CO | 5 | 432 ± 28 | 411 ± 31 | 411 ± 22 | 427 ± 25 | 399 ± 37 | 419 ± 11 |

BL, baseline; CO, carbon monoxide; 10% CO, top load of 10% blood volume of CO saturated saline; DMSO, dimethyl sulfoxide.
[a]$p < .05$ vs. baseline; [b]$p < .05$ vs. 10% top load.

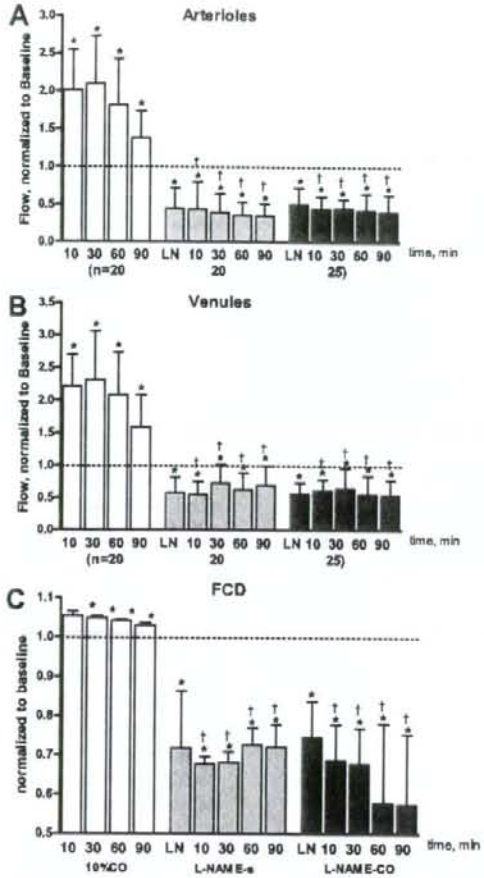


Figure 6. Changes of flow and functional capillary density (*FCD*) after L-NAME treatment (30 mg/kg$^{-1}$) in 10% carbon monoxide (*CO; white bars*), L-NAME followed by 10% blood volume saline top load (*L-NAME-s, gray bars*), and L-NAME followed by 10% blood volume CO-saline top load (*L-NAME-CO, black bars*). Broken line represents baseline level (BL). *A*, changes of arteriolar flow. Flow was decreased after L-NAME treatment; 10% CO-saline did not elicit the effects found in untreated hamsters (*$p < .05$ vs. BL, †$p < .05$ vs. CO-saline). *B*, changes of venular flow after L-NAME treatment. Flow was decreased after L-NAME treatment; 10% CO-saline did not elicit the effects (*$p < .05$ vs. BL, †$p < .05$ vs. CO-saline). *C*, changes of FCD after L-NAME treatment. FCD was decreased after L-NAME treatment; 10% CO-saline did not improve FCD (*$p < .05$ vs. BL, †$p < .05$ vs. CO-saline).

### CO Effect on Cardiac Output

CO increased cardiac output by 30% and flow in the window chamber by 100% (at 10% top load), indicating that not all tissues and organs responded uniformly to this stimulus. The mechanism responsible for this effect is not related to the activation of cGMP by CO, which has a negative inotropic effect on the heart. The principal factor increasing cardiac output should be afterload reduction resulting from vasodilation. An additional mechanism could be activation of $K_{ATP}$ channels, which can increase cardiac output after CO infusion (30, 31). Finally, microcirculatory effects may also take place in the heart muscle, improving cardiac perfusion and contractility.

### Effect of L-NAME and ODQ

The vasodilatory effect should be due to CO stimulating sGC (32) and increasing cGMP in vascular smooth muscle (33, 34) similarly to NO. NO can enhance activity of cGMP by a factor of 200–400, whereas CO has a maximal three-fold effect (35). Consequently, the CO effect on vasorelaxation is much smaller and about one thousandth that of NO (36); however, the effects of CO are longer lasting than those due to NO, which are in the time scale of minutes. The vasodilator effect of CO is concentration dependent and nonlinear, suggesting the presence of negative responses at the higher CO concentrations.

The vasodilatory effects of the infusion of CO-saline should share the same NO-sGC pathway as those due to endogenous CO, since pretreatment with the NOS inhibitor L-NAME and sGC inhibitor ODQ caused vasoconstriction (11, 37) and hypertension. In our study, L-NAME increased MAP and decreased HR, a result obtained also by Sakai et al. (11), whereas ODQ did not affect systemic variables in rats (38). DMSO vehicle did not affect either systemic or microvascular variables; thus, inhibition effect of CO was related to sGC inhibition by ODQ.

The most effective dosage of 10% CO-saline did not induce vasodilation after L-NAME injection and only partially after ODQ injection, suggesting that CO needs NO to cause vasodilation and that the sGC-cGMP pathway is not the only pathway causing vasodilation. cGMP independent pathways such as those associated with activating calcium-dependent $K^+$ channel (30, 31, 39) and the cytochrome P450-monogenase pathway (40, 41) may be involved. Also, both exogenous NO and endothelium-derived relaxing factor can cause vasodilatory effects by activating the $K^+$ channel without cGMP in rat aortic smooth muscle (42), although Trottier et al. (43) showed that activating cGMP independent pathway required higher concentration of NO (1–9 μM). Endothelium-derived relaxing factor acts exclusively through the cGMP pathway (43); thus, CO and NO interaction should be concentration dependent as suggested by Thoroup et al (15). CO and NO are interdependent in their regulation of vasoactivity (15, 16), and since NO production is present in the hamster window chamber (44, 45), CO is able to interfere with NO-mediated vasodilation (29). L-NAME and the sGC inhibitor ODQ abolish NO availability, rendering the activity of CO ineffective. Thus, our results are compatible with the hypothesis that CO stimulates the release of NO from an intracellular storage pool that is maintained in a dynamic state by NO generated by endothelial NOS (15).

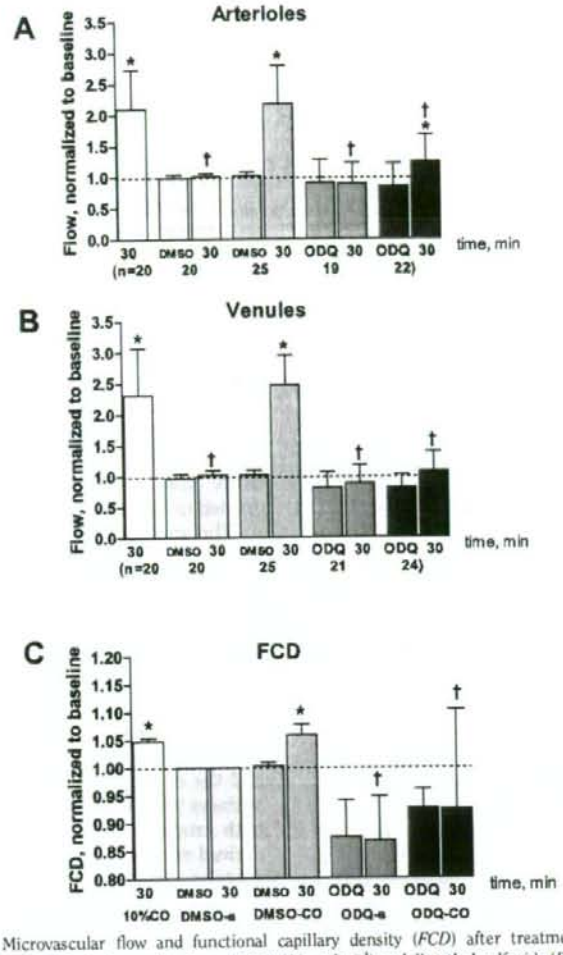


Figure 7. Microvascular flow and functional capillary density (*FCD*) after treatment with 1H-[1,2,4]oxadiazole[4,3-a]quinoxqalin-1-one (*ODQ*) (10 $\mu g \cdot kg^{-1}$) and dimethyl sulfoxide (*DMSO*) vehicle (0.04%) at 30 mins after saline or carbon monoxide (*CO*)-saline infusion: 10% CO-saline top load (*10% CO, white bars*), DMSO vehicle followed by saline top load (*DMSO-s, light gray bars*), DMSO vehicle followed by 10% CO-saline top load (*DMSO-CO, gray bars*), ODQ followed by saline top load (*ODQ-s, dark gray bars*), and ODQ followed by 10% CO-saline top load (*ODQ-CO, black bars*). Broken line represents baseline level (BL). *A*, changes of flow in arterioles. 10% CO increased flow at 30 mins after injection in arterioles (*$p < .05$ vs. BL) after DMSO and ODQ treatment; the magnitude of changes was smaller after ODQ treatment (†$p < .05$ vs. 10% CO). *B*, changes of flow in venules. 10% CO significantly increased flow in DMSO-CO group (*$p < .05$ vs. BL) but not after ODQ treatment (†$p < .05$ vs. 10% CO). *C*, changes of FCD. 0% CO increased flow at 30 mins after injection in arterioles (*$p < .05$ vs. BL) after DMSO treatment but not after ODQ treatment (†$p < .05$ vs. 10% CO).

### cGMP Content in the Chamber Window Tissue

cGMP increased in the 10% CO-saline group, showing that CO stimulates sGC-cGMP. Conversely, the 20% CO-saline group could not elicit vasorelaxation at 30 mins and did not change tissue cGMP content. Therefore, under NO availability conditions, CO causes a biphasic effect on local cGMP concentration (46). These phenomena indicate that CO stimulates the release of NO from an intracellular storage pool (15), and when CO concentration is sufficient it induces the release of preformed NO bound to heme proteins (47).

It is not evident from our study whether NO release by CO originates from preexisting intracellular pools or the stimulation of endothelial NOS. However, the intracellular pool would have to be rather large to sustain 90 mins duration of dilation (at 10% top load). Furthermore, the decline of the effect at 90 mins may also reflect the decrease in CO concentration as the gas diffuses out of the circulation.

Intravenous injection of CO-saturated saline is a novel method for delivering CO. Alternatives are intraperitoneal injection of CO gas (1), inhalation (1, 2, 48, 49), and the intravenous delivery of CO-releasing molecules (50, 51). Our approach provides a quantifiable delivery of CO with rapid and long-lasting hemodynamic effects. A limitation is that volume for infusion cannot be minimized because of the solubility of CO. Intraperitoneal injection of the gas has a delayed effect, and dosage may be less predictable due to the uncertainties related to the extent of anatomical diffusion barriers between the point of injection and uptake by the blood. Inhalation requires continuous delivery of the gas for >1 hr (2), and the effect may be complicated by toxicities at the level the lung. Finally, CO delivery by CO-releasing molecules does not have the hemodynamic effects noted in the present studies (50, 51) and primarily provides tissue protection when delivered before ischemic episodes.

## CONCLUSIONS

CO-saturated saline injection caused immediate vasodilation and increased blood flow in the hamster skin microcirculation, an effect that lasts as long as 90 mins. The effect is dose dependent and biphasic, since 10% BV of CO injection causes a maximal effect, whereas 2.5%, 5%, and 20% BV of CO-saline were not statistically different from baseline. This concentration of CO increased cardiac output by 30%. Pretreatment with the NOS inhibitor L-NAME completely abolished the CO effect, whereas pretreatment with the sGC inhibitor ODQ caused partial inhibition, which was confirmed by measurements of cGMP concentration in the tissues. These results indicate that CO-saline infusions are a practical method for introducing a therapeutic amount of CO into the circulation, which has a relatively long-lasting dilatory effect; however, dosage appears to be critical, since higher and lower dosages by a factor of two do not have any effect.

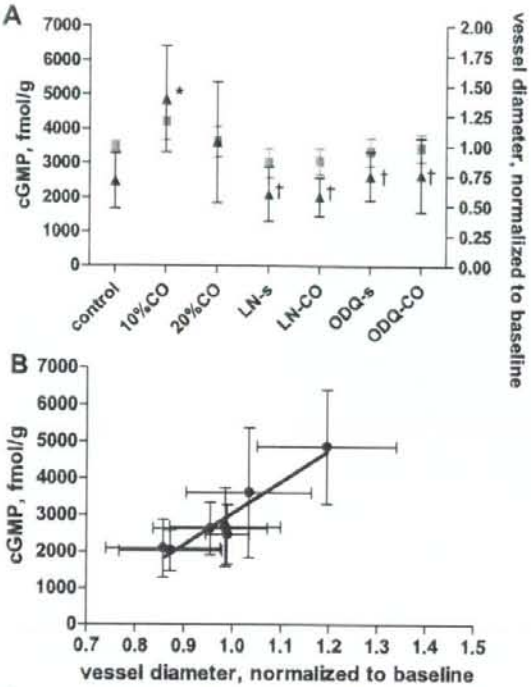


Figure 8. *A*, cyclic guanosine monophosphate (*cGMP*) concentration (*triangles*) and vessel diameter (*squares*) at 30 mins after saline or carbon monoxide (*CO*)-saline injection. cGMP in the 10% CO group was significantly higher than normal (*$p < .05$ vs. normal), L-NAME-treated, and 1H-[1,2,4]oxadiazole[4,3-a]quinoxqalin-1-one (*ODQ*)-treated groups (†$p < .05$ vs. 10% CO). *LN-s*, L-NAME followed by 10% blood volume saline top load; *LN-CO*, L-NAME followed by 10% blood volume CO-saline top load; *ODQ-s*, ODQ followed by saline top load; *ODQ-CO*, ODQ followed by 10% CO-saline top load. *B*, relation between cGMP concentration in the skin and changes of vessel diameter. There was significance between cGMP concentration and changes of diameter ($p < .05$, $R^2 = .92$).


## ACKNOWLEDGMENTS

We thank F. Barra and C. Walser for their expertise in performing the animal preparations used in this work.


## REFERENCES


1. Kanten WE, Penney DG, Francisco K, et al: Hemodynamic responses to acute carboxyhemoglobinemia in the rat. *Am J Physiol* 1983; 244:H320–H327
2. Gutierrez G, Rotman HH, Reid CM, et al: Comparison of canine cardiovascular response to inhaled and intraperitoneally infused CO. *J Appl Physiol* 1985; 58:558–563
3. Kerger H, Saltzman DJ, Menger MD, et al: Systemic and subcutaneous microvascular pO2 dissociation during 4-h hemorrhagic shock in conscious hamsters. *Am J Physiol* 1996; 270:H827–H836
4. Endrich B, Asaishi K, Götz A, et al: Technical report: A new chamber technique for microvascular studies in unanaesthetized hamsters. *Res Exp Med* 1980; 177:125–134
5. Intaglietta M, Silverman NR, Tompkins WR: Capillary flow velocity measurements in vivo and in situ by television methods. *Microvasc Res* 1975; 10:165–179
6. Lipowsky HH, Zweifach BW: Application of the "two-slit" photometric technique to the measurement of microvascular volumetric flow rates. *Microvasc Res* 1978; 15:93–101
7. Intaglietta M, Tompkins WR: Microvascular measurements by video image shearing and splitting. *Microvasc Res* 1973; 5:309–312
8. American College of Physicians: Practice Strategies for Elective Red Blood Cell Transfusion, Vol. 116. American College of Physicians, 1992
9. Parks J, Worth HGJ: Carboxyhemoglobin Determination by Second-Derivative Spectroscopy. *Clin Chem* 1985; 31:279–281
10. Cabrales P, Acero C, Intaglietta M, et al: Measurement of the cardiac output in small animals by thermodilution. *Microvasc Res* 2003; 66:77–82
11. Sakai H, Hara H, Tsai AG, et al: Constriction of resistance arteries determines L-NAME-induced hypertension in a conscious hamster model. *Microvasc Res* 2000; 60:21–27
12. Gimeno G, Carpentier PH, Desquand-Billiald S, et al: L-arginine and NG-nitro-L-arginine methyl ester cause macromolecule extravasation in the microcirculation of awake hamsters. *Eur J Pharmacol* 1998; 346:275–282
13. Panzali A, Signorini C, Albertini A: Improvement in lower carboxyhemoglobin range determination by second-derivative spectroscopy. *Clin Chem* 1987; 33:2311–2312
14. Guo Y, Stein AB, Wu WJ, et al: Administration of a CO-releasing molecule at the time of reperfusion reduces infarct size in vivo. *Am J Physiol Heart Circ Physiol* 2004; 286: H1649–H1653
15. Thorup C, Jones CL, Gross SS, et al: Carbon monoxide induces vasodilation and nitric oxide release but suppresses endothelial NOS. *Am J Physiol* 1999; 277:F882–F889
16. Kajimura M, Goda N, Suematsu M: Organ design for generation and reception of CO: Lessons from the liver. *Antioxid Redox Signal* 2002; 4:633–637
17. Imai T, Morita T, Shindo T, et al: Vascular smooth muscle cell-directed overexpression of heme oxygenase-1 elevates blood pressure through attenuation of nitric oxide-induced vasodilation in mice. *Circ Res* 2001; 89: 55–62
18. Klatt P, Schmidt K, Mayer B: Brain nitric oxide synthase is a haemoprotein. *Biochem J* 1992; 288:15–17
19. Matsuoka A, Stuehr DJ, Olson JS, et al: L-arginine and calmodulin regulation of the heme iron reactivity in neuronal nitric oxide synthase. *J Biol Chem* 1994; 269: 20335–20339
20. McMillan K, Masters BS: Prokaryotic expression of the heme- and flavin-binding domains of rat neuronal nitric oxide synthase as distinct polypeptides: Identification of the heme-binding proximal thiolate ligand as cysteine-415. *Biochemistry* 1995; 34: 3686–3693
21. Pufahl RA, Marletta MA: Oxidation of NG-hydroxy-L-arginine by nitric oxide synthase: evidence for the involvement of the heme in catalysis. *Biochem Biophys Res Commun* 1993; 193:963–970
22. White KA, Marletta MA: Nitric oxide synthase is a cytochrome P-450 type hemoprotein. *Biochemistry* 1992; 31:6627–6631
23. Johnson RA, Kozma F, Colombari E: Carbon monoxide: from toxin to endogenous modulator of cardiovascular functions. *Braz J Med Biol Res* 1999; 32:1–14
24. Willis D, Tomlinson A, Frederick R, et al: Modulation of heme oxygenase activity in rat brain and spleen by inhibitors and donors of nitric oxide. *Biochem Biophys Res Commun* 1995; 214:1152–1156
25. Durante W, Kroll MH, Christodoulides N, et al: Nitric oxide induces heme oxygenase-1 gene expression and carbon monoxide production in vascular smooth muscle cells. *Circ Res* 1997; 80:557–564
26. Ischiropoulos H, Beers MF, Ohnishi ST, et al: Nitric oxide production and perivascular nitration in brain after carbon monoxide poi-

soning in the rat. *J Clin Invest* 1996; 97: 2260–2267
27. Fan B, Wang J, Stuehr DJ, et al: NO synthase isozymes have distinct substrate binding sites. *Biochemistry* 1997; 36:12660–12665
28. McMillan K, Bredt DS, Hirsch DJ, et al: Cloned, expressed rat cerebellar nitric oxide synthase contains stoichiometric amounts of heme, which binds carbon monoxide. *Proc Natl Acad Sci U S A* 1992; 89:11141–11145
29. Ishikawa M, Kajimura M, Adachi T, et al: Carbon monoxide from heme oxygenase-2 Is a tonic regulator against NO-dependent vasodilatation in the adult rat cerebral microcirculation. *Circ Res* 2005; 97:e104–e114
30. Clark JE, Naughton P, Shurey S, et al: Cardioprotective actions by a water-soluble carbon monoxide-releasing molecule. *Circ Res* 2003; 93:e2–e8
31. Nishikawa Y, Stepp DW, Merkus D, et al: In vivo role of heme oxygenase in ischemic coronary vasodilation. *Am J Physiol Heart Circ Physiol* 2004; 286:H2296–H2304
32. Schmidt HH: NO, CO and OH. Endogenous soluble guanylyl cyclase-activating factors. *FEBS Lett* 1992; 307:102–107
33. Graser T, Vedernikov YP, Li DS: Study on the mechanism of carbon monoxide induced endothelium-independent relaxation in porcine coronary artery and vein. *Biomed Biochim Acta* 1990; 49:293–296
34. Marks GS, Brien JF, Nakatsu K, et al: Does carbon monoxide have a physiological function? *Trends Pharmacol Sci* 1991; 12: 185–188
35. Kharitonov VG, Sharma VS, Magde D, et al: Kinetics and equilibria of soluble guanylate cyclase ligation by CO: effect of YC-1. *Biochemistry* 1999; 38:10699–10706
36. Furchgott RF, Jothianandan D: Endothelium-dependent and -independent vasodilation involving cyclic GMP: relaxation induced by nitric oxide, carbon monoxide and light. *Blood Vessels* 1991; 28:52–61
37. Moro MA, Russel RJ, Cellek S, et al: cGMP mediates the vascular and platelet actions of nitric oxide: confirmation using an inhibitor of the soluble guanylyl cyclase. *Proc Natl Acad Sci U S A* 1996; 93:1480–1485
38. Cechova S, Pajewski TN: The soluble guanylyl cyclase inhibitor ODQ, 1H-[1,2,4]oxadiazolo[4,3-a]quinoxalin-1-one, dose-dependently reduces the threshold for isoflurane anesthesia in rats. *Anesth Analg* 2004; 99: 752–757
39. Wang R, Wu L, Wang Z: The direct effect of carbon monoxide on KCa channels in vascular smooth muscle cells. *Pflugers Arch* 1997; 434:285–291
40. Coceani F: Control of the ductus arteriosus—A new function for cytochrome P450, endothelin and nitric oxide. *Biochem Pharmacol* 1994; 48:1315–1318
41. Estabrook RW, Franklin MR, Hildebrandt AG: Factors influencing the inhibitory effect of carbon monoxide on cytochrome P-450-catalyzed mixed function oxidation reactions. *Ann N Y Acad Sci* 1970; 174:218–232
42. Bolotina VM, Najibi S, Palacino JJ, et al: Nitric oxide directly activates calcium-dependent potassium channels in vascular smooth muscle. *Nature* 1994; 368:850–853
43. Trottier G, Triggle CR, O'Neill SK, et al: Cyclic GMP-dependent and cyclic GMP-independent actions of nitric oxide on the renal afferent arteriole. *Br J Pharmacol* 1998; 125:563–569
44. Tsai AG, Acero C, Nance PR, et al: Elevated plasma viscosity in extreme hemodilution increases perivascular nitric oxide concentration and microvascular perfusion. *Am J Physiol Heart Circ Physiol* 2005; 288: H1730–H1739
45. Hangai-Hoger N, Nacharaju P, Manjula BN, et al: Microvascular effects following treatment with polyethylene glycol-albumin in lipopolysaccharide-induced endotoxemia. *Crit Care Med* 2006; 34:108–117
46. Ingi T, Cheng J, Ronnett GV: Carbon monoxide: An endogenous modulator of the nitric oxide-cyclic GMP signaling system. *Neuron* 1996; 16:835–842
47. Stamler JS, Piantadosi CA: O=O NO: It's CO. *J Clin Invest* 1996; 97:2165–2166
48. Fujimoto H, Ohno M, Ayabe S, et al: Carbon monoxide protects against cardiac ischemia-reperfusion injury in vivo via MAPK and Akt-eNOS pathways. *Arterioscler Thromb Vasc Biol* 2004; 24:1848–1853
49. Mazzola S, Forni M, Albertini M, et al: Inhaled carbon monoxide (CO) prevents lung oedema induced by endotoxic shock. *Vet Res Commun* 2004; 28(Suppl 1):209–212
50. Guo R, Gao XY, Wang W, et al: Tempol reduces reperfusion-induced arrhythmias in anaesthetized rats. *Pharmacol Res* 2005; 52: 192–198
51. Stein AB, Guo Y, Tan W, et al: Administration of a CO-releasing molecule induces late preconditioning against myocardial infarction. *J Mol Cell Cardiol* 2005; 38:127

Circulation Research
JOURNAL OF THE AMERICAN HEART ASSOCIATION

American Heart Association.
Learn and Live.

**Targeting NAD(P)H Oxidase: Ets-1 Regulates p47phox**

Takeshi Adachi, Michiko Yamamoto and Makoto Suematsu

*Circ. Res.* 2007;101;962-964
DOI: 10.1161/CIRCRESAHA.107.164434
Circulation Research is published by the American Heart Association. 7272 Greenville Avenue, Dallas, TX 72514
 Print ISSN: 0009-7330. Online ISSN: 1524-4571

*See related article, pages 985–994*

# Targeting NAD(P)H Oxidase
## Ets-1 Regulates p47$^{phox}$

Takeshi Adachi, Michiko Yamamoto, Makoto Suematsu

Reactive Oxygen Species (ROS) have been shown to modulate vascular signaling in endothelium, smooth muscle, and adventitia, regulate vascular hypertrophy, inflammation, remodeling, intracellular calcium, and disturb nitric oxide bioactivity.[1,2] Since Griendling et al discovered the activation of NAD(P)H oxidase by angiotensin II (Ang II),[3] researches have focused on the regulation of this enzyme in Ang II signaling/Ang II-induced hypertension both in vitro and in vivo. Vascular NAD(P)H oxidase consists of multiple subunits including p22$^{phox}$, p40$^{phox}$, p47$^{phox}$, p67$^{phox}$, Rac1, and unique catalytic subunits, Nox isoforms (gp91$^{phox}$ homologue).[4] The signaling mechanisms for the rapid activation of NAD(P)H oxidase by Ang II have been identified using cultured aortic vascular smooth muscle cells (VSMCs). Ang II rapidly activates PLC to increase intracellular calcium and diacylglycerol levels, which causes the activation of protein kinase C (PKC). PKC phosphorylates p47$^{phox}$ and releases ROS from Nox subunits. Subsequently, ROS activates cSrc, EGF-receptor, PI3-kinase, and Rac1, leading to the secondary activation of NAD(P)H oxidase to augment the intracellular ROS levels.[4] These events occur within 30 minutes in cultured VSMCs. Considering the ROS generation associated with hypertension in vivo, the latter transcriptional upregulation of NAD(P)H oxidase subunits by Ang II might be more important. Ang II upregulates the expressions of NAD(P)H oxidase subunits after more than 4 hours including p22$^{phox}$, Nox2 (gp91$^{phox}$), p47$^{phox}$, and p67$^{phox}$,[5] however the mechanisms of transcriptional regulations for NAD(P)H oxidase subunits have not fully been elucidated yet.

In this issue of *Circulation Research*, Ni and colleagues identified that Ets-1 was a critical transcriptional regulator of p47$^{phox}$ induced by Ang II in vitro and in vivo.[6] Ets-1 has been known as a proto-oncogene transcription factor to induce matrix-degradation proteins such as collagenase, plasminogen activation inhibitor-1(PAI-1), and matrix-metalloproteinases. Ets-1 can be induced by TNF-$\alpha$, endothelin-1, prostanoid(s), and platelet-derived growth factor,[7–8] suggesting an implication in vascular inflammation. Indeed, this group previously reported that Ets-1 was a critical factor needed to induce cyclin-dependent kinase, PAI-I, vascular cells adhesion molecule-1, and monocyte chemoattractant protein-1 in response to Ang II. In Ets-1$^{-/-}$ mice, the vascular inflammation by Ang II infusion, which was represented by the recruitment of T cell and macrophage to vessel wall, was blunted, although hypertensive response was preserved.[9] In this article, the authors carefully seek the molecular mechanisms to regulate the expression of NAD(P)H oxidase subunits by Ets-1. The augmentation of superoxide and hydrogen peroxide ($H_2O_2$) generations by Ang II were markedly attenuated in aorta from Ets-1$^{-/-}$ mice or VSMCs with siRNA for Ets-1. siRNA for Ets-1 also blunted the upregulation of p47$^{phox}$ without affecting the expression of Nox1, Nox4, Rac1, p22$^{phox}$, and p67$^{phox}$ by Ang II. They used gel-shift assay, luciferase reporter assay, and chromatin immunoprecipitation assay with deletion mutant of p47$^{phox}$ promoter, and identified the −45 Ets-1–binding promoter region as essential for the induction of p47$^{phox}$. They developed peptides to inhibit ETS-1 bindings (DN-Ets-1 peptides) and delivered them to the Ang II–infused mice in vivo. DN-Ets-1 peptides attenuated medial hypertrophy and aortic ROS generation without affecting hypertensive response to Ang II.

This article impacts the field of hypertension research in 3 major ways. First, the authors demonstrate the importance of p47$^{phox}$ induction for aortic ROS generation in Ang II–induced hypertension. p47$^{phox}$ is phosphorylated at S359/S370/S379 by PKC, which causes association with p22$^{phox}$. S303/S304 of p47$^{phox}$ were also phosphorylated to augment the catalytic activity of NAD(P)H oxidase.[4] We expressed S303A/S304A mutant p47$^{phox}$ in VSMCs to suppress the redox-sensitive signal by Ang II.[10] The posttranslational modifications of p47$^{phox}$ by Ang II are critical for the rapid activation of NAD(P)H oxidase.

The importance of p47$^{phox}$ expression in Ang II–induced hypertension was also shown by Landmesser and colleagues.[11] An increase in superoxide generation of aorta by Ang II was blunted in p47$^{phox-/-}$ mice but rose 3-fold in control. Hypertensive response to Ang II was modestly decreased in p47$^{phox-/-}$ mice. Consistent with these observations and the results by Ni and colleagues,[6] p47$^{phox}$ induction is essential for aortic ROS generation and vascular inflammation in Ang II-infusion, whereas it is not required for the hypertensive response. Because Ets-1 is a critical transcriptional regulator for p47$^{phox}$, it is a potential therapeutic target for vascular inflammation.

Second, this study showed the importance of transcriptional regulation of the NAD(P)H oxidase. The authors clearly show the specific induction of p47$^{phox}$ by Ets-1 without affecting the expressions of other subunits by Ang II. AP-1 was shown to regulate the expression of p67$^{phox}$ in



From the Department of Biochemistry and Integrative Medical Biology, School of Medicine, Keio University, Tokyo, Japan.

Correspondence to Takeshi Adachi, MD, PhD, Department of Biochemistry and Integrative Medical Biology, School of Medicine, Keio University, Research Park 4N8, 35 Shinanomachi Shinjuku-ku, Tokyo Japan 160-8582. E-mail tadachi@sc.itc.keio.ac.jp

(*Circ Res.* **2007;101:962-964.**)



***Circulation Research* is available at http://circres.ahajournals.org**
**DOI: 10.1161/CIRCRESAHA.107.164434**

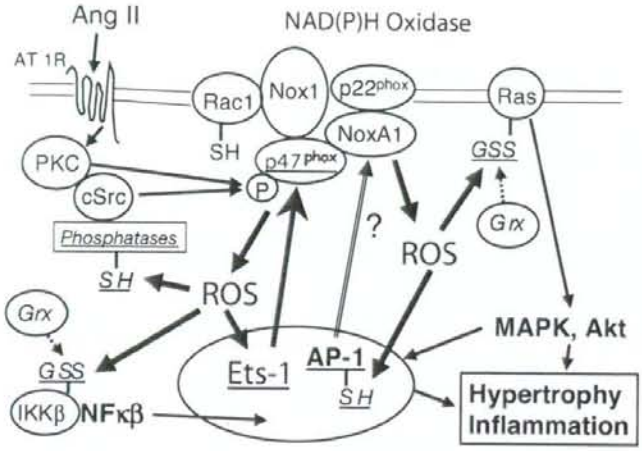


**Figure.** Targeting NAD(P)H oxidase. The mechanism to regulate NAD(P)H oxidase by Ang II is shown. PKC and c-Src activates NAD(P)H oxidase with the phosphorylation of $p47^{phox}$. Ets-1 upregulates $p47^{phox}$ expression. ROS from NADPH oxidase can modify thiols on the multiple target proteins and Trx/Grx reverses them. There are various strategies for targeting NAD(P)H oxidase in the system, including unique subunits, kinases/phosphatases, small GTPases, thiol-mediated regulations, and transcription factors.

monoytes,[12] however, vascular NAD(P)H oxidase may contain an alternative to $p67^{phox}$ subunit, NoxA1,[4] and the transcriptional regulation of vascular NAD(P)H oxidases are largely unknown. Stimulation of VSMCs with Ang II activates many of early genes, including AP-1 (c-fos, c-jun), NF-$\kappa\beta$(p50, p65), ATF/CREB, hypoxia-inducible factor-1 (HIF-1), Egr-1, STAT1, and Nrf-2.[1,13] Wilson et al[14] showed that $H_2O_2$ upregulated translations of Ets-1, which were mediated by the activation of Nrf-2/ARE (antioxidant response element). It is possible that the rapid activation of NADPH oxidase causes the expression of Ets-1 by redox-sensitive mechanism, which in turn induces $p47^{phox}$ for the booster effects of ROS generation by Ang II.

## Redox-Sensitive Thiols Can Be Critical Targets for NAD(P)H Oxidase

Although the molecular mechanisms for the redox-sensitive signaling are not fully known, growing evidence indicates the importance of thiols modification by ROS.[15] ROS can modify the redox-sensitive thiols to sulfenylation (RSOH), sulfinylation ($RSO_2H$), and S-glutathiolation (RSSG). We previously found that Ang II increased ROS generation from NAD(P)H oxidase, which caused the activation of Ras via S-glutathiolation at Cys118 in VSMCs. Because many of the oncogene/transcription factors can be upregulated by the activation of Ras, the mechanism may be implicated in the ROS-mediated transcriptional regulations.[1,10] There are several other candidates for thiol-containing proteins targeted by ROS. Phosphatases have critical redox-sensitive thiols in the center of catalytic sites and the oxidation of them by ROS decreases their activity.[16] Rac1 contains a redox-sensitive thiol to modulate its function.[17] Caspase can be inhibited by S-glutathiolation,[18] and Thioredoxin (Trx) and glutaredoxin (Grx) can reverse thiol-modifications of Ras, phosphatases, and caspases.[10,15,18] Interestingly, another Trx superfamily, protein disulfide isomerase, is associated with NAD(P)H oxidase and supports ROS generation.[19] Transcriptional factors can be also regulated by ROS via redox-sensitive thiols. Cys179 on IKK$\beta$ is S-glutathiolated by ROS from Nox1, which causes NF-$\kappa\beta$ activation.[20] ROS oxidizes the reactive thiol on Keap1 to dissociate Nrf-2, leading to the Nrf-2-transcription. In contrast, many transcription factors such as AP-1 and NF-$\kappa\beta$ have redox-sensitive thiols in the DNA-binding sites and their modifications disturb DNA binding. The effects of ROS on transcription may differ according to the localization of ROS.[13]

## Targeting NAD(P)H Oxidase for Vascular Diseases

Third, the authors used unique peptides to block Ets-1 transcription for in vivo models. DN-Ets-1 peptides contained HIV-TAT protein membrane-transduction domains to promote intracellular delivery, especially to the nucleus. In the past, Pagano and colleagues generated gp91-ds-tat peptides, which inhibited the interaction between Nox2 and $p47^{phox}$ and efficiently decreased vascular ROS from NAD(P)H oxidase.[21] Similar peptide drugs may be useful for targeting proteins related with NAD(P)H oxidase. With recent advances for understanding the regulation of NAD(P)H oxidase, we can create multiple strategies to modulate NAD(P)H oxidase activity (Figure). The AT1 receptor blocker attenuates Ang II signaling. Statin, a HMG-CoA reductase inhibitor, decreases farnysyl/geranylgeranyl pyrophosphate, leading to the suppression of Ras/Rac1.[22] Inhibition of glucose 6-phosphate dehydrogenase decreases intracellular NADPH and ROS from NAD(P)H oxidase,[23] although it may weaken the antioxidant defenses. Many of the redox-sensitive thiols and thiol-reducing enzymes (Trx/Grx/PDI) can be the downstream targets.[15] Moreover, redox-sensitive transcriptional factors can be new targets for the suppression of NAD(P)H oxidase.

## Sources of Funding

The work was supported by Grants-in-Aid for Scientific Research (B:19390090) (to T.A.) and for Creative Scientific Research 17GS0419 (to T.A. and M.S.). T.A. and M.S. are core members of Global Center-of-Excellence (GCOE) for Human Metabolomics Systems Biology from MEXT. M.Y. is a research fellow supported by New Energy and Industrial Technology Development Organization.

## Disclosures

None.

## References


1. Griendling KK, Sorescu D, Lassegue B, Ushio-Fukai M. Modulation of protein kinase activity and gene expression by reactive oxygen species and their role in vascular physiology and pathophysiology. *Arterioscler Thromb Vasc Biol.* 2000;20:2175–2183.
2. Suzuki H, DeLano FA, Parks DA, Jamshidi N, Granger DN, Ishii H, Suematsu M, Zweifach BW, Schmid-Schoenbein GW. Xanthine oxidase activity associated with arterial blood pressure in spontaneously hypertensive rats. *Proc Natl Acad Sci U S A.* 1998;95:4754–4759.
3. Griendling KK, Minieri CA, Ollerenshaw JD, Alxander RW. Angiotensin II stimulates NADH and NADPH oxidase activity in cultured vascular smooth muscle cells. *Circ Res.* 1994;74:1141–1148.
4. Lyle AN, Griendling KK. Modulation of vascular smooth muscle signaling by reactive oxygen species. *Physiology.* 2006;21:269–280.
5. Touyz RM, Chen X, Tabet F, Yao G, He G, Quinn MT, Pagano PJ, Schiffrin EL. Expression of a functional active gp91phox-containing neutrophil-type NAD(P)H oxidase in smooth muscle cells from human resistance arteries: regulation by angiotensin II. *Circ Res.* 2002;90:1205–1213.
6. Ni W, Zhan Y, He H, Maynard E, Balschi JA, Oettgen P. Est-1 is a critical transcriptional regulator of reactive oxygen species and $p47^{phox}$ gene expression in response to angiotensin II. *Circ Res.* 2007;101:985–994.
7. Naito S, Shimizu S, Maeda S, Wang J, Paul R, Fagin JA. Ets-1 is an early response gene activated by ET-1 and PDGF-BB in vascular smooth muscle cells. *Am J Physiol.* 1998;274:C472–C480.
8. Ito H, Duxbury M, Benoit E, Clancy TE, Zinner MJ, Ashley SW, Whang EE. Prostagrandin E2 enhances pancreatic cancer invasiveness through an Ets-1-dependnet induction of matrix metalloproteinase-2. *Cancer Res.* 2004;64:7439–7446.
9. Zhan Y, Brown C, Maynard E, Anshelevich A, Ni W, Ho IC, Oettgen P. Ets-1 is a critical regulator of Ang II-mediated vascular inflammation and remodeling. *J Clin Invest.* 2005;115:2508–2516.
10. Adachi T, Pimentel DR, Heibeck T, Hou X, Lee YJ, Jiang B, Ido Y, Cohen RA. S-glutathiolation of Ras mediates redox-sensitive signaling by angiotensin II in vascular smooth muscle cells. *J Biol Chem.* 2004;279:29857–29862.
11. Landmesser U, Cai H, Dikalov S, McCann L, Hwang J, Jo H, Holland SM, Harrison DG. Role of p47phox in vascular oxidative stress and hypertension caused by angiotensin II. *Hypertension.* 2002;40:511–515.
12. Gauss KA, Bunger PL, Quinn MT. Ap-1 is essential for p67(phox) promotor activity. *J Leuckoc Biol.* 2002;71:163–172.
13. Liu H, Colavitti R, Rovira II, Finkel T. Redox-dependent transcriptional Regulation. *Circ Res.* 2005;97:967–974.
14. Wilson LA, Gemin A, Espiritu R, Singh G. ets-1 is transcriptionally up-regulated by $H_2O_2$ via an antioxidant response element. *FASEB J.* 2005;19:2085–2087.
15. Adachi T, Schöneich C, Cohen RA. S-Glutathiolation in redox-sensitive signaling. *Drug Discov Today.* 2005;2:39–46.
16. Rhee SG, Bae YS, Lee SR, Kwon J. Hydrogen peroxide: a key messenger that modulates protein phosphorylation through cysteine oxidation. *Sci STKE.* 2000;2000:PE1.
17. Heo J, Campbell SL. Mechanism of redox-mediated guanine nucleotide exchange on redox-activate Rho GTPase. *J Biol Chem.* 2005;280:31003–31010.
18. Pan S, Berk BC. Glutathiolation regulates tumor necrosis factor-alpha-induced caspase-3 cleavage and apoptosis: key role for glutaredoxin in the death pathway. *Circ Res.* 2007;100:213–219.
19. Janiszewski M, Lopes LR, Carmo AO, Pedro MA, Brandes RP, Santos CX, Laurindo FR. Regulation of NAD(P)H oxidase by associated protein disulfide isomerase in vascular smooth muscle cells. *J Biol Chem.* 2005;280:40813–40819.
20. Reynaert NL, van der Vliet A, Guala AS, McGovern T, Hristova M, Pantano C, Heintz NH, Heim J, Ho YS, Matthews DE, Wouters EF, Janssen-Heininger YM. Dynamic redox control of NF-kappaB through glutaredoxin-regulated S-glutathionylation of inhibitory kappaB kinase beta. *Proc Natl Acad Sci U S A.* 2006;103:13086–13091.
21. Rey FE, Cifuentes ME, Kiarash A, Quinn MT, Pagano PJ. Novel competitive inhibitor of NAD(P)H oxidase assembly attenuates vascular $O_2^-$ and systolic blood pressure in mice. *Circ Res.* 2001;89:408–414.
22. Ito M, Adachi T, Pimentel DR, Ido Y, Colucci WS. Statin inhibit beta-adrenergic receptor-stimulated apoptosis in adult rat ventricular myocyte via a Rac1-dependent mechanism. *Circulation.* 2004;110:412–418.
23. Matsui R, Xu S, Maitland KA, Hayes A, Leopold JA, Handy DE, Loscalzo J, Cohen RA. Glucose-6 phosphate dehydrogenase deficiency decreases the vascular response to angiotensin II. *Circulation.* 2005;112:257–263.


KEY WORDS: Ets-1 ■ NAD(P)H oxidase ■ Angiotensin II ■ hypertension

0022-3565/08/3251-69–76.00
THE JOURNAL OF PHARMACOLOGY AND EXPERIMENTAL THERAPEUTICS

JPET 325:69–76, 2008

Vol. 325, No. 1
132100/3322647
*Printed in U.S.A.*

# Design and Evaluation of *S*-Nitrosylated Human Serum Albumin as a Novel Anticancer Drug

Naohisa Katayama, Keisuke Nakajou, Hisakazu Komori, Kunitoshi Uchida, Jun-ichi Yokoe, Norikiyo Yasui, Hisashi Yamamoto, Toshiya Kai, Makoto Sato, Takenobu Nakagawa, Motohiro Takeya, Toru Maruyama, and Masaki Otagiri

*Departments of Biopharmaceutics (N.K., H.K., T.K., M.O.) and Clinical Pharmaceutics (T.M.), Graduate School of Pharmaceutical Sciences, and Department of Cell Pathology (T.N., M.T.), Graduate School of Medical Sciences, Kumamoto University, Kumamoto, Japan; and Pharmaceutical Research Center, Nipro Corporation, Shiga, Japan (N.K., K.N., K.U., J.-i.Y., N.Y., H.Y., T.K., M.S.)*

Received September 26, 2007; accepted January 23, 2008

**ABSTRACT**

In recent studies, the cytotoxic activity of NO has been investigated for its potential use in anticancer therapies. Nitrosated human serum albumin (NO-HSA) may act as a reservoir of NO in vivo. However, there are no published reports regarding the effects of NO-HSA on cancer. Therefore, the present study investigated the antitumor activity of NO-HSA. NO-HSA was prepared by incubating HSA, which had been sulfhydrylated using iminothiolane, with isopentyl nitrite (6.64 mol NO/mol HSA). Antitumor activity was examined in vitro using murine colon 26 carcinoma (C26) cells and in vivo using C26 tumor-bearing mice. Exposure to NO-HSA increased the production of reactive oxygen species in C26 cells. Flow cytometric analysis using rhodamine 123 showed that NO-HSA caused mitochondrial depolarization. Activation of caspase-3 and DNA fragmentation were observed in C26 cells after incubation with 100 $\mu$M NO-HSA for 24 h, and NO-HSA inhibited the growth of C26 cells in a concentration-dependent manner. The growth of C26 tumors in mice was significantly inhibited by administration of NO-HSA compared with saline and HSA treatment. Immunohistochemical analysis of tumor tissues demonstrated an increase in terminal deoxynucleotidyl transferase dUTP nick-end labeling-positive cells in NO-HSA-treated mice, suggesting that inhibition of tumor growth by NO-HSA was mediated through induction of apoptosis. Biochemical parameters (such as serum creatinine, blood urea nitrogen, aspartate aminotransferase, and alanine aminotransferase) showed no significant differences among the three treatment groups, indicating that NO-HSA did not cause hepatic or renal damage. These results suggest that NO-HSA has the potential for chemopreventive and/or chemotherapeutic activity with few side effects.

Although cancer primarily arises from disorders of cell proliferation, it also may arise from disruptions in programmed cell death signaling pathways, resulting in decreased apoptosis of cancerous cells (Okada and Mak, 2004). Therefore, induction of apoptosis in neoplastic cells is a very effective therapy for tumor eradication (Meng et al., 2006). However, this type of chemotherapy often has negative side effects, such as transient cell cycle arrest, senescence, and autophagy. Drug delivery systems that facilitate selective apoptosis of neoplastic cells have been suggested as a way of overcoming this problem (Kaufmann and Gores, 2000; Kondo et al., 2005).

NO is a unique diffusible molecular messenger that occupies a central role in mammalian pathophysiology (Brune et al., 1998). Its multiple actions include vascular smooth muscle relaxation (Moncada et al., 1986; Ignarro, 1989), inhibition of platelet aggregation (Azuma et al., 1986), effects on neurotransmission (Garthwaite, 1991), and regulation of immune function (Marletta et al., 1988). Alternatively, under some circumstances, NO is cytotoxic (Laval and Wink, 1994). NO causes cellular iron losses and inhibits DNA synthesis, mitochondrial respiration, and aconitase activity in L10 hepatoma cells (Hibbs et al., 1988). In addition, NO reacts with

Article, publication date, and citation information can be found at http://jpet.aspetjournals.org.
doi:10.1124/jpet.107.132100.

**ABBREVIATIONS:** NSAID, nonsteroidal anti-inflammatory drug; ASA, aspirin; HSA, human serum albumin; DTPA, diethylenetriaminepentaacetic acid; HBSS, Hanks' balanced salt solution; rHSA, recombinant human serum albumin; PAGE, polyacrylamide gel electrophoresis; C26, murine colon 26 carcinoma; ROS, reactive oxygen species; PBS, phosphate-buffered saline; CM-$H_2$DCFDA, 5-(and-6)-chloromethyl-2′,7′-dichlorodihydrofluorescein diacetate, acetyl ester; TUNEL, terminal deoxynucleotidyl transferase dUTP nick-end labeling; Cr, serum creatinine; BUN, blood urea nitrogen; ALT, alanine aminotransferase; AST, aspartate aminotransferase; ALP, alkaline phosphatase; BSA, bovine serum albumin; GSNO, *S*-nitrosoglutathione; R410C, genetic variant of human serum albumin mutated at position 410.

superoxide anion (which is produced by activated macrophages and other cells), to form peroxynitrite. This by-product of NO is a potent chemical oxidant, which alters protein function and damages DNA (Beckman and Crow, 1993). These effects are part of the nonspecific host defense, which facilitates killing of tumor cells and intracellular pathogens. In addition, the cytotoxicity arising from long-lasting NO generation has been attributed to induction of apoptosis (Brune et al., 1998).

In recent studies, the cytotoxic activity of NO has been studied to assess its therapeutic potential in cancer treatment. NO-donating nonsteroidal anti-inflammatory drugs (NSAIDs), especially NO-aspirin (NO-ASA), have been investigated as promising chemopreventive agents (Williams et al., 2001; Kashfi et al., 2002; Fabbri et al., 2005). NO-ASA consists of traditional ASA to which an NO-releasing moiety is bound via a spacer. This agent induces oxidative stress by increasing intracellular peroxide and $O_2^-$, thereby inducing apoptosis via activation of the intrinsic apoptosis pathway (Gao et al., 2005). JS-K is a prodrug designed to release NO after reacting with glutathione transferase, which induces double-stranded DNA breaks, activates DNA damage response pathways, and induces apoptosis in human multiple myeloma cells both in vitro and in vivo (Kiziltepe et al., 2007).

Human serum albumin (HSA) is an abundant circulating protein, and the nitrosated form serves as a reservoir of NO (Stamler et al., 1992). Therefore, NO-HSA is an NO donor that is currently being investigated for its potential therapeutic applications. For example, administration of NO-HSA to animals with ischemia-reperfusion injury minimizes the tissue damage that occurs after reperfusion (Semsroth et al., 2005). In a balloon-injured rabbit femoral artery model, locally delivered NO-HSA preferentially binds to sites of vessel injury and inhibits both platelet accumulation and the subsequent development of neointimal hyperplasia (Marks et al., 1995). NO-HSA also shows potent antibacterial activity and inhibits the proliferation of cultured human vascular smooth muscle cells (Ishima et al., 2007). However, there are no reports describing the effects of NO-HSA on cancer.

Accordingly, the present study evaluated the antitumor activity of NO bound to HSA (NO-HSA) via an *S*-nitrosothiol linkage using iminothiolane as a spacer. The molecular events related to induction of apoptosis by NO-HSA were studied in vitro, and the antitumor activity of NO-HSA was studied in vivo using a murine model of C26 colon carcinoma.

## Materials and Methods

**Chemicals.** Traut's reagent (2-imminothiolane) was purchased from Pierce Chemical (Rockford, IL). Isopentyl nitrite, diethylenetriaminepentaacetic acid (DTPA), and Cell Counting Kit-8 (WST-8) were purchased from Wako Pure Chemicals (Osaka, Japan). RPMI 1640 medium, Hanks' balanced salt solution (HBSS), and RNase A were obtained from Sigma-Aldrich (St. Louis, MO). Proteinase K was obtained from Roche Applied Science (Indianapolis, IN). All other reagents used were of the highest grade available from commercial sources.

**Expression and Purification of Recombinant HSA.** rHSA was produced using a yeast expression system as described previously (Matsushita et al., 2004). In brief, for constructing the HSA expression vector pPIC9-HSA, native HSA coding region was incorporated into the methanol-inducible pPIC9 vector (Invitrogen, Carlsbad, CA). The resulting vector was introduced into the yeast species *Pichia pastoris* (strain GS115) to express rHSA. Secreted rHSA was isolated from the growth medium by a combination of precipitation with 60% (w/v) $(NH_4)_2SO_4$ and purification on a Blue Sepharose CL-6B column (GE Healthcare, Little Chalfont, Buckinghamshire, UK) followed by Phenyl HP column (GE Healthcare). Isolated protein was defatted by using the charcoal procedure described by Chen (1967), deionized, freeze-dried, and then stored at −20°C until use. The resulting rHSA (treated with dithiothreitol) exhibited a single band on SDS-PAGE. Density analysis of protein bands stained with Coomassie Brilliant Blue showed that its purity was more than 97%.

**Synthesis of NO-HSA.** Terminal sulfhydryl groups were added to the HSA molecule by incubating 0.15 mM rHSA with 3 mM Traut's reagent in 100 mM potassium phosphate buffer containing 0.5 mM DTPA, pH 7.8, for 1 h at room temperature. The resultant modified rHSA then was *S*-nitrosylated by 3-h incubation with 15 mM isopentyl nitrite at room temperature (Fig. 1). The resulting NO-HSA was concentrated, exchanged with saline using a PelliconXL filtration device (Millipore Corporation, Billerica, MA), and the final concentration adjusted to 2 mM NO-HSA. The sample was stored at −80°C until use.

**Determination of S-Nitrosylation Efficiency.** The amount of the *S*-nitroso moieties of NO-HSA was quantified using a 96-well plate. First, 20-μl aliquots of NO-HSA solution and $NaNO_2$ (standard) were incubated with 0.2 ml of 10 mM sodium acetate buffer, pH 5.5, containing 100 mM NaCl, 0.5 mM DTPA, 0.015% *N*-1-naphthylsthylene-diamide and 0.15% sulfanilamide with or without 0.09 mM $HgCl_2$, for 30 min at room temperature. Then, the absorbance was measured at 540 nm. The number of moles of NO per mole of HSA was obtained by subtracting the values in the absence of $HgCl_2$ from values in the presence of $HgCl_2$; the value thus obtained, was 6.64 ± 0.54 mol NO/mol HSA.

**Cellular Experiments with C26 Cells.** C26 cells, which were donated by the Institute of Development, Aging and Cancer, at Tohoku University (Sendai, Miyagi, Japan), were cultured at 37°C in RPMI 1640 medium containing 10% fetal calf serum, 100 U/ml penicillin, and 10 μg/ml streptomycin (medium A). Trypsin (0.25%) EDTA solution was used to detach the cells from the culture flask for plating and passing the cells. All cell culture experiments were performed at 37°C in a humidified atmosphere of 5% $CO_2$ in air.

For detection of reactive oxygen species (ROS), C26 cells ($1.0 \times 10^4$ cells/well) were cultured in 96-well plates in medium A for 12 h, they were washed twice with PBS, and then they were incubated for an additional 30 min in HBSS containing 5 μM 5-(and-6)-chloromethyl-2',7'-dichlorodihydrofluorescein diacetate, acetyl ester (CM-$H_2$DCFDA) (Invitrogen, Carlsbad, CA). After washing twice with HBSS, the cells were cultured in HBSS containing 5% fetal calf serum for 15 min followed by the addition of PBS, 50 μM HSA, or 50 μM NO-HSA. After incubation, fluorescence was measured using a plate reader (excitation wavelength, 485 nm; emission wavelength, 535 nm). The change in fluorescence was calculated by subtracting the fluorescence at 0 h from the fluorescence measured at the indicated times. The fluorescence intensities of cells incubated with PBS, 50 μM HSA, and 50 μM NO-HSA at 0 h were 201.3, 166.1, and 181.3, respectively.

Changes in the mitochondrial membrane potential of C26 cells

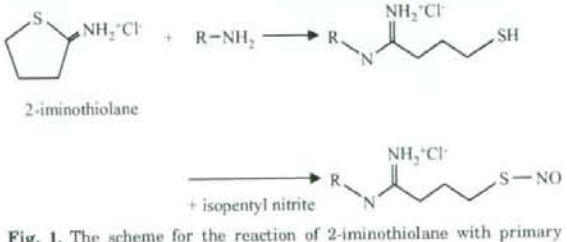


**Fig. 1.** The scheme for the reaction of 2-iminothiolane with primary amines followed by *S*-nitrosylation.

were monitored using flow cytometric analysis with rhodamine 123 staining. C26 cells ($1.0 \times 10^6$ cells/well) were cultured in six-well plates for 12 h, washed twice with PBS, and incubated with PBS and either 100 $\mu$M HSA or various concentrations of NO-HSA in medium A for 24 h. The cells were then trypsinized, washed twice with PBS, and incubated for 15 min with 5 $\mu$g/ml rhodamine 123. The mean fluorescence intensity of rhodamine 123 in the cells was measured using a flow cytometer (FACSCalibur; BD Biosciences, Franklin Lakes, NJ).

For the determination of caspase-3 activity, cells were cultured to confluence in six-well plates, washed twice with PBS, and incubated with medium A containing 100 $\mu$M HSA or various concentrations of NO-HSA. Cells were incubated for 24 h, trypsinized, and washed with 0.2 ml of ice-cold PBS. The cell pellet was resuspended in 15 $\mu$l of cell lysis buffer, it was lysed by freeze-thawing, and then it was incubated on ice for 15 min. The cell lysates were centrifuged at 15,000 rpm for 20 min at 4°C, and the supernatant fraction was collected (cell extract). The caspase-3 activity in the cell extract was assessed using the colorimetric CaspASE Assay System (Promega, Madison, WI), according to the manufacturer's instructions.

For the detection of DNA degradation (DNA ladder), C26 cells ($1.0 \times 10^6$ cell/well) were cultured in six-well plates. Cells were cultured for 12 h, they were washed twice with PBS, and then they were incubated with PBS and either 100 $\mu$M HSA or various concentrations of NO-HSA for 24 h. The cells then were trypsinized, collected, and centrifuged at 4000 rpm for 10 min. After removing the supernatant, the cell pellet was resuspended in 0.2 ml of PBS, and then it was centrifuged at 4000 rpm for 10 min. The supernatant was again removed, and the remaining pellet was incubated in 20 $\mu$l of 10 mM Tris-HCl buffer, pH 7.8, containing 2 mM EDTA and 0.5% SDS (cell lysis buffer) for 10 min at 4°C, followed by centrifugation at 15,000 rpm for 5 min. The resulting supernatant (cell extract) was collected and incubated with 1 $\mu$l of RNase A (10 $\mu$g/ml) for 30 min at 50°C. One microliter of proteinase K (10 $\mu$g/ml) was added to the cell extract, followed by a 1-h incubation at 50°C. The resulting DNA extract was electrophoresed in a 2.0% agarose gel, followed by staining of the gel with ethidium bromide and visualization of the DNA bands using ultraviolet illumination.

The cell viability assay was performed using WST-8, which is based on the 3-(4,5-dimethylthiazol-2-yl)-2,5-diphenyltetrazolium assay. C26 cells were plated in 96-well plates at $1.0 \times 10^4$ cells/well, and they were cultured for 32 h in medium A. Then, the cells were washed twice with PBS and incubated in a total volume of 0.2 ml of medium A containing various concentrations of HSA or NO-HSA. After incubating the cultures for various lengths of time, 5 $\mu$l of WST-8 solution was added to each well, and the cells were incubated for an additional 2 h at 37°C. The number of surviving cells was determined by measuring the absorbance at 450 nm. Cell viability was calculated as the percentage of the control value (without HSA or NO-HSA) (Ishiyama et al., 1996).

**Animal Experiments.** Five-week-old male BALB/c AnNCrlCrlj mice (17–20 g) were purchased from Charles River Italica (Calco, Italy). The mice were housed in a 12-h light/dark cycle in a humidity-controlled room. Mice were acclimated for at least 5 days before being used in experiments.

For tumor induction, mice were inoculated with C26 cells ($1.0 \times 10^6$ cells/mouse) by a subcutaneous injection into the dorsal skin. Three days after inoculation, C26 carcinoma-bearing mice were randomly divided into three groups: control, HSA, and NO-HSA. The mice received a daily i.v. injection of saline, HSA (10 $\mu$mol/kg), or NO-HSA (10 $\mu$mol/kg) for 10 days from day 3 to day 12 after inoculation. Tumor volume was calculated using the formula $0.4\ (a \times b^2)$, where a is the largest diameter and b is the smallest diameter of the tumor (Shimizu et al., 2005), and volume was monitored from day 7 to day 17 after inoculation. Variance in each group was evaluated using the Bartlett test, and differences in mean tumor volume were evaluated using the Tukey-Kramer test.

Some animals in each of the three treatment groups were used for immunohistochemical analysis and serum biochemistry. When the mice received five times per day from day 3 to day 7 after inoculation (the tumors in each group reached approximately 5 mm in diameter), blood samples were collected from the abdominal vena cava under diethyl ether anesthesia approximately 2 h after the daily injection, and then the mice were sacrificed.

Tumors were dissected, they were fixed immediately with 2% periodate/lysine/paraform-aldehyde fixative at 4°C for 5 h, and then they were washed with a graded series of sucrose solutions in PBS (10, 15, and 20%). After immersion in 20% sucrose in PBS to inhibit ice crystal formation, the tissues were embedded in O.C.T. compound (Sakura Fine Technochemical, Tokyo, Japan), they were frozen in liquid nitrogen, and then they were stored at −80°C. Five-micrometer tumor sections were prepared using a cryostatic microtome (HM500M; Microm, Walldorf, Germany), and they were mounted on poly-L-lysine-coated slides. The slides were stained using the TUNEL method and an in situ apoptosis detection kit (Takara-Bio Co. Ltd., Shiga, Japan). The slides were washed three times with 0.01 M phosphate buffer, pH 7.4, containing 0.9% NaCl, followed by application of methanol containing 0.3% $H_2O_2$ to inactivate endogenous peroxidase and incubation at room temperature for 30 min. The slides were washed 3 times with 0.01 M phosphate-buffered saline, and then they were incubated in 100 ml of permeabilization buffer on ice for 5 min. The slides were washed three times with 0.01 M phosphate-buffered saline, and then they were incubated with 50 ml of freshly prepared terminal deoxynucleotidyl transferase reaction mixture (5 ml of terminal deoxynucleotidyl transferase enzyme + 45 ml of Labeling Safe buffer) at 37°C for 60 min. After the slides were washed three times with 0.01 M PBS, they were incubated in 70 ml of anti-fluorescein isothiocyanate-horseradish peroxidase conjugate antibody at 37°C for 30 min. After the slides were washed three times with 0.01 M PBS, they were incubated in 3,3-diaminobenzidine-$H_2O_2$ reaction buffer at room temperature for 10 min. After the slides were washed three times with distilled water, they were stained with 3% methyl green for 10 min, dehydrated, penetrated, and sealed (Gavrieli et al., 1992). Each slide then was visualized under a light microscope (Olympus, Tokyo, Japan), at a magnification of 400×.

Serum was separated by centrifugation. Routine clinical laboratory techniques were used to determine the concentrations of total protein, serum creatinine (Cr), blood urea nitrogen (BUN), alanine aminotransferase (ALT), aspartate aminotransferase (AST), and alkaline phosphatase (ALP) in serum. Variance in each group was evaluated using the Bartlett test, and differences were evaluated using the Tukey-Kramer test.

## Results

**NO-HSA Induces Cell Death via Apoptosis in Vitro.** Apoptosis is induced by a variety of factors. Among them, it is well known that intracellular accumulation of ROS, such as $H_2O_2$, $O_2^-$, and peroxynitrite, causes apoptosis. Moreover, production of ROS also plays a major role in NO-ASA-induced apoptosis. To examine whether NO-HSA promoted ROS production in C26 cells, a fluorescent probe (CM-$H_2$DCFDA), which undergoes conversion to 2′,7′-dichlorofluorescein in the presence of intracellular ROS, was used. Addition of NO-HSA to C26 cells increased the amount of ROS compared with treatment with vehicle or HSA (Fig. 2). In addition, the ROS in the C26 cell culture medium increased with time after addition of NO-HSA. This result suggests that NO-HSA promotes a signal cascade leading to apoptosis by increasing intracellular production of ROS.

To evaluate the effect of NO-HSA on mitochondrial function, C26 cells were loaded with a mitochondria-selective fluorescent cation (rhodamine 123) to monitor the mitochon-

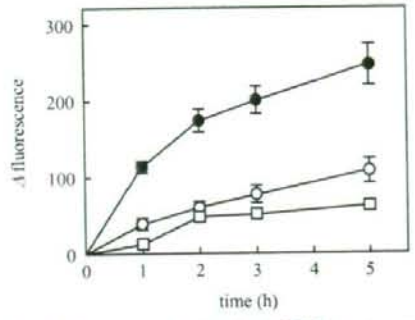


**Fig. 2.** Production of ROS in C26 cells after NO-HSA treatment. C26 cells were pretreated with CM-$H_2$DCFDA for uptake into C26 cells and hydrolysis by cellular esterase, followed by addition of either PBS (open circles), 50 $\mu$M HSA (open squares), or 50 $\mu$M NO-HSA (closed circles). Excitation of the probes was done at 485 nm, and emission was measured at 535 nm. Change in fluorescence was calculated by subtracting the fluorescence at 0 h from that at the indicated times. The fluorescence intensities of the PBS, 50 $\mu$M HSA, and 50 $\mu$M NO-HSA groups at 0 h were 201.3, 166.1, and 181.3, respectively. Results are the mean ± S.D. of three separate experiments.

drial membrane potential. Compared with vehicle, in cells treated with 50 or 100 $\mu$M NO-HSA rhodamine 123, fluorescence was decreased by 75%, whereas treatment with 25 $\mu$M NO-HSA or 100 $\mu$M HSA did not affect rhodamine 123 fluorescence compared with vehicle (Fig. 3A). These observations indicate that NO-HSA induces depolarization of the mitochondrial membrane.

Caspase-3 is a cell death protease that is involved in the downstream execution phase of apoptosis. During this phase of apoptosis, cells undergo morphological changes, such as DNA fragmentation, chromatin condensation, and formation of apoptotic bodies. Compared with the effect of vehicle, cells treated with 25 or 50 $\mu$M NO-HSA had slightly increased caspase-3 activity, and cells treated with 100 $\mu$M NO-HSA showed a larger increase in caspase-3 activity (Fig. 3B). Cells treated with HSA had the same level of caspase-3 activity as cells treated with PBS.

To further confirm that NO-HSA induced apoptosis in C26 cells, DNA fragmentation, which is a typical morphological change in the execution phase of apoptosis, was examined. DNA fragmentation was observed in C26 cells treated with 100 $\mu$M NO-HSA, but not in C26 cells treated with 25 or 50 $\mu$M NO-HSA (Fig. 3C). Neither vehicle nor 100 $\mu$M HSA induced DNA fragmentation in C26 cells (Fig. 3C). These findings suggest that NO-HSA induces apoptosis by increasing ROS production, activating caspase-3, and hyperpolarizing the mitochondrial membrane potential.

To determine the effect of NO-HSA on cell growth, the viability of C26 cells was examined after treatment with HSA or various concentrations of NO-HSA. NO-HSA inhibited growth of C26 cells in a concentration-dependent manner; cell growth was suppressed by 71, 80, and 85% after a 48-h incubation with 25, 50, and 100 $\mu$M NO-HSA, respectively (Fig. 4A). The viability of C26 cells incubated with 50 $\mu$M NO-HSA significantly decreased with increasing incubation times (Fig. 4B). NO-HSA inhibited growth to a greater extent than did HSA, which had only a weak inhibitory effect. These results suggest that NO-HSA inhibits cell growth of C26 cells by inducing apoptosis.

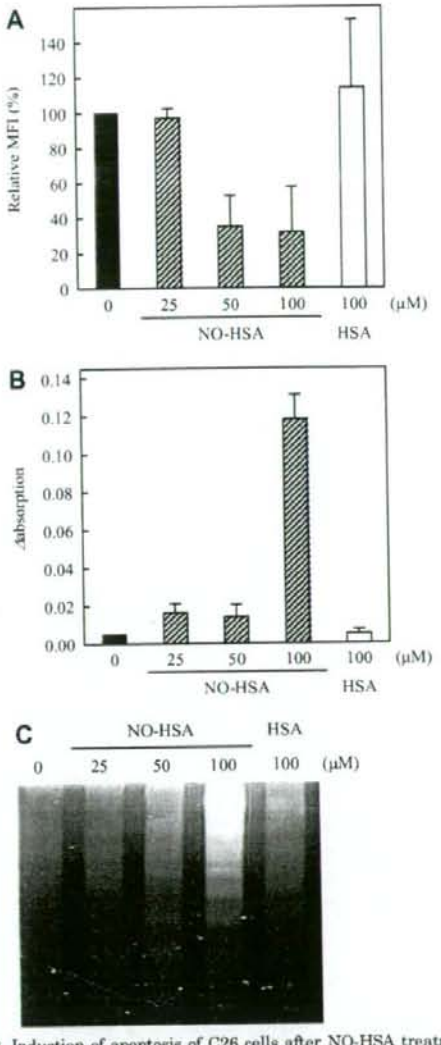


**Fig. 3.** Induction of apoptosis of C26 cells after NO-HSA treatment. A, alteration in the mitochondrial membrane potential after NO-HSA treatment. C26 cells were cultured with PBS, 100 $\mu$M HSA, or various concentrations of NO-HSA for 24 h, followed by addition of rhodamine 123. The amounts of cell-associated rhodamine 123 were determined as described under *Materials and Methods*. Results are the mean ± S.D. of three separate experiments. B, activation of caspase-3 after NO-HSA treatment. C26 cells were incubated with PBS, 100 $\mu$M HSA, or various concentrations of NO-HSA for 24 h. Caspase-3 activity was estimated by monitoring *p*-nitroaniline (absorbance at 405 nm) released from the substrate upon cleavage by caspase-3. Change in absorbance was calculated by subtracting absorbance after incubation with caspase inhibitor (*N*-benzyloxycarbonyl-Val-Ala-Asp-fluoromethylketone), from absorbance after incubation without caspase inhibitor. The absorbances among PBS-, HSA- and NO-HSA-treated cells incubated with *N*-benzyloxycarbonyl-Val-Ala-Asp-fluoromethylketone were almost identical (0.170 ± 0.17). Results are the means ± S.D. of three separate experiments. C, DNA fragmentation after NO-HSA treatment. C26 cells were incubated with PBS, 100 $\mu$M HSA or various concentrations of NO-HSA for 24 h. DNA fragmentation was detected as described under *Materials and Methods*.

**NO-HSA Exerts Antitumor Effect via the Apoptotic Pathway in Vivo.** To investigate the antitumor effect of NO-HSA in vivo, C26 tumor-bearing mice received i.v. injec-

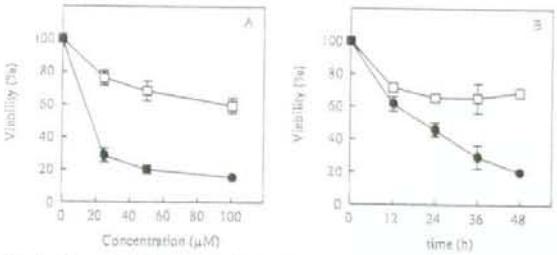


**Fig. 4.** Effect of NO-HSA on C26 cell viability. A, C26 cells were treated for 48 h with various concentrations of HSA (open squares) or NO-HSA (closed circles). B, C26 cells were incubated for the indicated times with 100 μM HSA (open squares) or 100 μM NO-HSA (closed circles). Cell viability was determined as described under *Materials and Methods*. Results are the mean ± S.D. of three separate experiments.

tions with saline, HSA, or NO-HSA. Mean tumor area increased with time in the saline-treated group. In the HSA-treated group, tumor growth was suppressed, compared with that in the control group, but the difference was not statistically significant. In contrast, tumor growth was significantly inhibited by administration of NO-HSA (Fig. 5).

To clarify whether the suppression of tumor growth by NO-HSA is mediated via apoptosis, tumor tissues from C26 tumor-bearing mice receiving injections with NO-HSA were examined using immunohistochemistry. In NO-HSA-treated mice, there were more TUNEL-positive cells than in the saline- and HSA-treated animals. In addition, the tumor tissue architecture was less defined in animals treated with NO-HSA than in the other groups, suggesting that NO-HSA induced apoptosis in C26 tumor cells and thus exerted an antitumor effect in vivo (Fig. 6).

To evaluate the side effects of NO-HSA treatment, several serum biochemical parameters were measured in tumor-bearing mice treated with saline, HSA, or NO-HSA (Table 1). There were no significant differences in total protein, Cr, BUN, AST, or ALT among the three groups, suggesting that

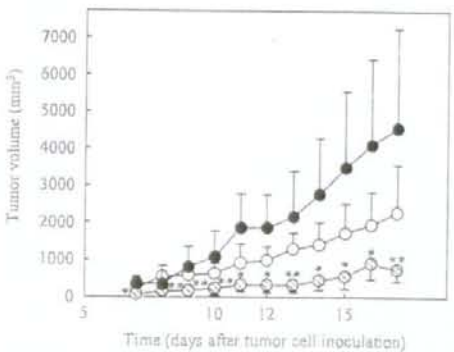


**Fig. 5.** Effect of NO-HSA on tumor growth in C26 tumor-bearing mice. C26 tumor-bearing mice were given daily i.v. injections of saline (5 ml/kg), HSA (10 μmol/5 ml/kg), or NO-HSA (10 μmol/5 ml/kg) for 10 days from day 3 to day 12 after inoculation with tumor cells. Tumor size was measured and tumor volume was calculated according to the formula, $V = 0.4a^2b$, where $a$ is the smallest, and $b$ is the largest, superficial diameter. Results are means ± S.D., $n = 10$ animals per experimental group. *, statistically significant reduction compared with saline ($P < 0.01$) or HSA ($P < 0.05$) at the corresponding time. **, statistically significant reduction compared with saline ($P < 0.01$) or HSA ($P < 0.01$) at the corresponding time.

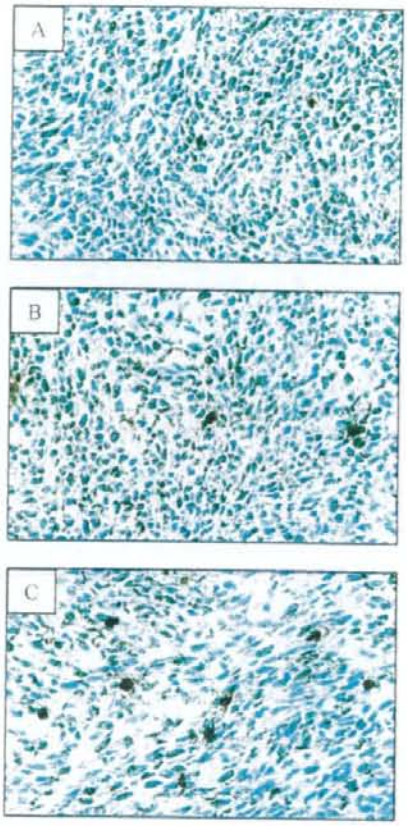


**Fig. 6.** Immunohistochemical staining of tumor tissues of C26 tumor-bearing mice receiving i.v. injections with NO-HSA using the TUNEL method. C26 tumor-bearing mice were given daily i.v. injections of saline (5 ml/kg) (A), HSA (10 μmol/5 ml/kg) (B), or NO-HSA (10 μmol/5 ml/kg) (C) for 5 days from day 3 to day 7 after inoculation with tumor cells. TUNEL staining, performed as described under *Materials and Methods*, shows apoptotic cells in the tumor tissue of mice treated with NO-HSA.

TABLE 1

Serum biochemical parameters of C26 tumor-bearing mice treated with saline, HSA, or NO-HSA

C26 tumor-bearing mice received i.v. injections five times per day with saline (5 ml/kg), HSA (10 μmol/5 ml/kg), or NO-HSA (10 μmol/5 ml/kg) from day 3 to day 7 after inoculation with tumor cells. Blood samples were collected from the abdominal vena cava under anesthesia with diethyl ether approximately 2 h after the last treatment injection, and mice were sacrificed. Serum biochemical parameters were measured using routine clinical laboratory techniques.

| Serum Biochemical Parameter | Saline | HSA | NO-HSA |
|---|---|---|---|
| Total protein (g/dl) | 5.23 ± 0.21 | 5.33 ± 0.06 | 5.55 ± 0.24 |
| Cr (mg/dl) | 0.13 ± 0.04 | 0.14 ± 0.01 | 0.16 ± 0.01 |
| BUN (mg/dl) | 15.25 ± 0.96 | 15.33 ± 1.53 | 13.75 ± 1.26 |
| AST (U/l) | 143.5 ± 62.9 | 91.7 ± 39.4 | 116.3 ± 69.1 |
| ALT (U/l) | 169.8 ± 111.6 | 110.0 ± 81.2 | 161.3 ± 126.2 |
| ALP (U/l) | 385.3 ± 18.3 | 345.3 ± 4.7* | 300.5 ± 23.0**,† |

* $P < 0.05$, saline vs. HSA.
** $P < 0.01$, saline vs. NO-HSA.
† $P < 0.05$, HSA vs. NO-HSA.

NO-HSA did not cause kidney or liver damage. However, compared with the control group, mice treated with HSA had significantly lower serum levels of ALP (345.3 ± 4.7 versus 385.3 ± 18.3 U/l). Moreover, the serum concentration of ALP

in mice treated with NO-HSA was 300.5 ± 23.0 U/l, which was significantly lower than the control ($P < 0.01$) and HSA ($P < 0.05$) groups. In general, ALP levels increase in several types of cancer, such as liver, lung, and bone cancer; thus, the present findings suggest that NO-HSA is an effective anticancer agent. The vasodilating effect of NO-HSA was also evaluated in rats after i.v. injection at a dose of 10 μmol/kg (66 μmol of NO per kg). NO-HSA induced a decrease in the mean arterial blood pressure immediately after i.v. injection and the maximum reduction effect was 32.8 ± 7.3 mm Hg. In contrast, HSA had no significant effect on the blood pressure. The fall in pressure returned to the initial levels in 30 min (data not shown).

## Discussion

There have been many trials of NO as a therapeutic agent, because of its powerful biological activity (Moncada and Higgs, 1993). However, the in vivo half-life of NO (~0.1 s) is often too short to capitalize on its potential biological actions. The half-life of NO can be prolonged by adding *S*-nitrosothiol moieties with cysteine residues of proteins. For example, nitrosated HSA seems to act as a reservoir of NO in vivo (Stamler et al., 1992). Simon et al. (1996) incubated bovine serum albumin (BSA) with 200-fold excess concentration of $NaNO_2$ under acidic condition to synthesize polynitrosylated BSA that is highly modified at the thiol group of cysteine, hydroxyl group of tyrosine and amines (38 mol NO/mol BSA). The polynitrosylated BSA has been shown to exhibit antiplatelet activity. However, polynitrosylated *S*-NO-BSA, an NO-BSA conjugate prepared with the same method except that the BSA has been reduced with dithiothreitol and it contains 19 mol of "*S*-NO" per mol of BSA, was a significantly more potent platelet inhibitor than polynitrosylated BSA described above. These findings show that nitrosylated BSA behaves as an NO donor; in particular, the poly(*S*-nitroso) derivative could be by far the most potent compound. One molecule of HSA contains 35 cysteine residues, 34 of which form 17 nonreactive disulfide bonds, and one of which (Cys-34) forms a reactive free thiol (Peters, 1985). Thus, the number of NO molecules that can be bound to HSA is limited because only one free cysteine per HSA molecule is available for conjugation. Ewing et al. increased the number of free sulfhydryl groups on BSA by reduction with dithiothreitol and thiolation with *N*-acetylhomocysteine, thereby preparing polynitrosated BSA (12–15 mol NO/mol BSA) (Ewing et al., 1997). Marks et al. (1995) produced polynitrosated BSA (5.9 mol NO/mol BSA) by adding free sulfhydryl groups to the molecule and by treating the BSA with *N*-acetylhomocysteine thiolactone. However, the polynitrosated BSAs prepared in these studies formed aggregates as a result of intermolecular disulfide formation. Aggregate formation results in molecular heterogeneity, which limits the therapeutic application of *S*-nitroso residues. In the present study, iminothiolane, which reacts with primary amines to introduce sulfhydryl groups while maintaining charge properties similar to the original amino groups, was selected as the thiolation reagent. Iminothiolane was used to produce polynitrosated HSA (NO-HSA) (6.6 mol NO/mol HSA), which did not form aggregates after nonreducing SDS-PAGE or native-PAGE (data not shown). Moreover, the far-UV CD spectra of NO-HSA were nearly identical to those of HSA (data not shown). Therefore, NO-HSA is expected to be clinically applicable as a biocompatible pharmacological agent, although further study is required to clarify other potential issues, including the antigenicity of this protein.

NO-NSAIDs have been extensively investigated as therapeutic agents for cancer due to their ability to release NO, thereby promoting apoptosis. NO-NSAIDs are categorized as organic nitrate esters, which are readily reduced to organic nitrite esters by cytosolic enzymes. Subsequently, glutathione reacts with organic nitrite esters to form GSNO, indicating that NO-NSAIDs release NO via *S*-nitrosothiol (Wong and Fukuto, 1999). Alternatively, the transfer of NO from NO-HSA to the cytosol could be inferred from a study by Ramachandran et al. (2001). They reported that NO is released from extracellular *S*-nitrosothiols by a cell surface enzyme (protein disulfide isomerase) and that it accumulates in the cell membrane where it reacts with $O_2$ to produce $N_2O_3$, which is then available for nitrosation reactions with intracellular thiols at the membrane-cytosol interface (Ramachardran et al., 2001). Therefore, it is possible that NO-HSA also releases NO by the intracellular formation of *S*-nitrosothiol, suggesting that the species of NO released within the cell by *S*-nitrosothiols, as well as the reactive substances (such as ROS) derived from the released NO, would not differ significantly between NO-NSAIDs and NO-HSA. In support of this hypothesis, NO-HSA caused depolarization of the mitochondrial membrane potential, activation of caspase-3 and DNA fragmentation in the present study, consistent with the effects of NO-NSAIDs. Additional studies are needed to determine the details of the molecular events and the systematic pathways affected by NO-HSA, but the mechanism of action should be similar to that of NO-NSAIDs. In a recent study, Gao et al. (2005) elucidated the detailed mechanism of apoptosis induced by NO-ASA. Intracellular accumulation of ROS is a key proximal event in NO-ASA-induced apoptosis, and it correlates with the effect on tumor cell growth (Gao et al., 2005). In the present study, NO-HSA induced accumulation of ROS in tumor cells, suggesting that increased ROS production may be an important proximal event leading to induction of apoptosis.

The results of the in vivo study showed that NO-HSA significantly suppressed tumor growth by inducing apoptosis, without adverse changes in serum biochemical parameters in treated mice. In a recent study, Trachootham et al. (2006), using immortalized cell lines and their oncogenic progeny transfected with *H-Ras*$^{V12}$, demonstrated that cancer cells typically produce more ROS than normal cells. Moreover, the pro-oxidant status of cancer cells increases their susceptibility to treatment with agents that cause oxidative stress, as demonstrated in a study using β-phenylethyl isothiocyanate (Trachootham et al., 2006). In addition, Feng et al. (2007) reported that cyaniding-3-rutinoside selectively induces accumulation of peroxides in HL-60 human leukemic cells, but not in normal peripheral blood mononuclear cells (Feng et al., 2007). Schumacker (2006) has proposed that ROS toxicity induced by certain chemotherapeutic agents may be an effective means of selectively eradicating malignant cells. In the present study, we presumed that although NO reacts with superoxide anion to form peroxynitrite (a potent oxidant and nitrating agent), these highly reactive oxidant species are probably produced at higher